Analysis of threshold effects in ultracold atomic collisions

Frederick H. Mies
Atomic Physics Division, National Institute of Standards and Technology, Gaithersburg, Maryland 20899

Maurice Raoult
Laboratoire de Photophysique Moléculaire, Université Paris XI, 91405 Orsay Cedex, France

(Received 20 January 2000; published 14 June 2000)

At the ultracold temperatures which occur in cold atom traps and Bose-Einstein condensates, only a few partial waves contribute to the scattering of ground-state alkali-metal atoms, and cross sections are extremely sensitive to threshold effects. We present an analysis of these threshold effects, using a generalized multichannel quantum defect theory (GMQDT) to construct a close-coupled scattering wave function which is analytic in energy across thresholds. We illustrate the theory using the hyperfine transitions in Na+Na collisions, and show that it gives results completely equivalent to the usual close-coupled cross sections. The virtue of the GMQDT is that it treats both open and closed channels on an equal footing, and all interchannel dynamics is summarized in a single real symmetric matrix $\mathbf{Y}(E)$ which is essentially constant across thresholds (and often over excursions of energy which exceed the hyperfine splittings). The multichannel threshold energy behavior can then be related to calculable properties of the individual channels that are being closed. Many of the smaller spin depolarization cross sections are determined by very long-range α^2/R^3 spin-spin interactions which are not well treated by GMQDT, and we correct these specific elements with a perturbative distorted-wave approximation which yields the observed threshold dependences and brings the GMQDT into perfect agreement with the exact close-coupled results.

PACS number(s): 34.10.+x, 34.50.−s, 34.20.Cf

I. INTRODUCTION

Collisions between ultracold atoms [1–7] have been observed and calculated at temperatures below 1 mK. These differ from ''normal'' collisions at $T \gg 1$ K in several significant ways. The long-time and distance scales associated with ultracold collisions enhance the importance of weak interactions such as those associated with hyperfine couplings [1–5] or external magnetic [6] or optical fields [7]. Moreover, only a few partial waves contribute to the cross sections, and the dynamics become extremely sensitive to threshold effects.

Our analysis of threshold effects is derived from a generalized version of multichannel quantum defect theory (GMQDT) previously developed to describe the dissociation of diatomic molecules [8–12]. We will use as a case study the collision-induced hyperfine transitions

$$\mathrm{Na}(3s,f_a,m_a)+\mathrm{Na}(3s,f_b,m_b) \rightarrow \mathrm{Na}(3s,f_a',m_a')+\mathrm{Na}(3s,f_b',m_a') \qquad (1.1)$$

of ground-state Na atoms at temperatures on the order of 1 μK. For the ^{23}Na isotope, the nuclear spin $I=\frac{3}{2}$ combined with the $S=\frac{1}{2}$ electronic spin of the ground state Na($3s\ ^2S$) atom yields two hyperfine angular momenta states $f_a=1$ and 2 which are split by 0.059095 cm^{-1} or equivalently 85.024 mK. This splitting is huge compared to the incident relative kinetic energy $\varepsilon \approx 1$ μK, and the energy released in an exothermic collision is sufficient to eject the atoms from ultracold traps [1–5]. Such binary loss mechanisms are often a major deterrent to achieving Bose-Einstein condensation. The detailed close-coupled (CC) description of these collisions, and the interactions that are required to induce them, are discussed in Sec. II.

The goal of GMQDT is to represent the exact solutions of the close-coupled scattering equations in a form that is an analytic function of the total collision energy E, especially as we cross some threshold at, say $E=0$, where a subset of channels can open or close. A real, symmetric, energy-insensitive matrix $\mathbf{Y}$ is defined which completely and exactly summarizes all the dynamics that we have managed to include in our close-coupled expansion of the scattering wave functions. In this paper we present numerical algorithms, based on a Milne analysis [10–12] of each channel contributing to the scattering, which directly evaluates $\mathbf{Y}$. At a given E the set of $N=N_O+N_C$ channels included in the close-coupled equations include N_O open and N_C closed channels, and the $N\times N$ matrix $\mathbf{Y}$ blocks into open and closed subsets

$$\mathbf{Y}=\begin{bmatrix}\mathbf{Y}_{OO} & \mathbf{Y}_{OC}\\ \mathbf{Y}_{CO} & \mathbf{Y}_{CC}\end{bmatrix}. \qquad (1.2)$$

This will be used to define a physically meaningful (observable) $N_O\times N_O$ scattering matrix $\mathbf{S}_{OO}(E)$ which is completely equivalent to that obtained from the usual CC equations.

It must be emphasized that the complete physics of the scattering problem is already dictated by the $N\times N$ interaction matrix $W_{i,j}(R)$ that is used in solving the close-coupled equations. The goal of GMQDT is not so much to add any new physics, but rather to add new insight into the dynamics by representing these *same exact* solutions to the resultant set of CC scattering equations in a form that is an analytic function of the total energy E. As described in Sec. III, the $\mathbf{Y}(E)$ matrix has no intrinsic meaning by itself, but rather is *defined by our choice of reference potentials* $V_j(R)$ and the resultant pair of independent reference wave functions $f_j(E,R)$ and $g_j(E,R)$ that we assign to each of the channel states $|j\rangle$ that

 ©2000 The American Physical Society

are included in the expansion of the multichannel continuum wave function $\Psi_i^+ = \Sigma_j |j\rangle F_{j,i}(R)/R$ incident in channel $|i\rangle$. If we are careful in choosing an appropriate set of N reference potentials, and take care to define reference functions which are properly analytic in E, we can insure that the matrix $\mathbf{Y}(E)$ is also analytic in energy, and can be safely extrapolated across thresholds. Generally we can choose reference potentials which insure that $\mathbf{Y}(E)$ is a slowly varying function of E, and often essentially a constant $\mathbf{Y}(E) \approx \mathbf{Y}(0)$ throughout the threshold region [8,9].

Let us first consider the case when all open channels are *appreciably* above threshold. From the analytic asymptotic properties of the individual reference functions $f_j(E,R)$ and $g_j(E,R)$ we obtain an energy-dependent elastic scattering phase shift $\xi_j(E)$ for each open channel $j=1, N_O$ and an energy dependent bound-state phase $\nu_j(E)$ for each closed channel $j=N_O+1,N$. Given the matrix $\mathbf{Y}$ and the diagonal $N_O \times N_O$ matrix of elastic scattering phase shifts $\xi_O(E)$ and the diagonal $N_C \times N_C$ matrix of bound-state phases $\nu_C(E)$ the scattering matrix is given by the expression [8]

$$\mathbf{S}_{OO}(E) = e^{+i\xi_O(E)}[1+i\overline{\mathbf{Y}}_{OO}(E)][1-i\overline{\mathbf{Y}}_{OO}(E)]^{-1}e^{+i\xi_O(E)}, \tag{1.3}$$

where $\overline{\mathbf{Y}}_{OO}(E)$ incorporates any resonance structure caused by coupling to closed channels, and can be appreciably energy dependent due to its dependence on the bound state phase $\nu_C(E)$:

$$\overline{\mathbf{Y}}_{OO}(E) = \mathbf{Y}_{OO} - \mathbf{Y}_{OC}[\tan \nu_C(E) + \mathbf{Y}_{CC}]^{-1}\mathbf{Y}_{CO}. \tag{1.4}$$

At first glance, one can see how GMQDT recovers the energy variation of the multichannel $\mathbf{S}_{OO}(E)$ through the energy dependence of the single-channel QDT parameters $\xi_O(E)$ and $\nu_C(E)$. Resonances are approximately located at the poles of the matrix $[\tan \nu_C(E) + \mathbf{Y}_{CC}]^{-1}$, where the zeros of the bound-state phase $\tan \nu_C(E) = 0$ locate the bound-state eigenvalues in the closed channels, and $\mathbf{Y}_{CC}$ introduces shifts in the resonance positions induced by the close coupling. We generally refer to such closed-channel resonances as Feshbach resonances. This analytic behavior is one of the salient features of the GMQDT approach to close-coupling phenomena, and has been amply demonstrated in many cases [8–11] not involving thresholds. In the special case when *all* channels are closed the determinant condition $|\tan \nu_C(E_n) + \mathbf{Y}_{CC}| = 0$ exactly locates the eigenvalues E_n for the close-coupled bound states [8,9] of the diatom. The detailed structure of both shape and closed-channel (Feshbach) resonances, as well as pure bound states in the vicinity of thresholds is especially interesting and will be presented in a subsequent paper.

In this paper we want to demonstrate the advantage of using the GMQDT approach in analyzing many interesting aspects of multichannel threshold phenomena, especially as it impacts on the physics of ultracold atom-atom collisions. Basically, the validity of Eq. (3) requires that the WKB-like boundary conditions that we use to define the open-channel reference functions in the classically assessible regions at short range actually persists out to infinity where we extract $\mathbf{S}_{OO}$. As we approach threshold this condition is violated and we need to introduce a second set of reference functions s_O and c_O with WKB-like boundary conditions set in the asymptotic region. This introduces two additional energy-sensitive QDT parameters $C_O(E)$ and $\tan \lambda_O(E)$ which give an analytic connection between the short-range (f_O, g_O) and long-range (s_O, c_O) sets of reference functions. The multichannel effects of these parameters are introduced by defining a modified matrix $\overline{\mathbf{R}}_{OO}(E)$ in place of $\overline{\mathbf{Y}}_{OO}(E)$ in Eq. (3),

$$\mathbf{S}_{OO}(E) = e^{+i\xi_O(E)}[1+i\overline{\mathbf{R}}_{OO}][1-i\overline{\mathbf{R}}_{OO}]^{-1}e^{+i\xi_O(E)}, \tag{1.5}$$

where

$$\overline{\mathbf{R}}_{OO}(E) = C_O(E)^{-1}[\overline{\mathbf{Y}}_{OO}^{-1} - \tan \lambda_O(E)^{-1}]C_O(E)^{-1}. \tag{1.6}$$

Specifically, the $C_O(E)$ parameter connects the amplitude between the functions f_O and s_O, both of which are well behaved as $R \to 0$. The departure of $C_O(E)$ from 1 measures the magnitude of the deviation from the WKB approximation. As the WKB approximation relies on a phase-amplitude approximation, a change in C_O generally leads to a change in phase. The $\tan \lambda_O(E)$ parameter accounts for this modification in phase, and its deviation from 0 also means a departure from WKB behavior. Note that well above threshold the parameters approach $\tan \lambda_O(E) \to 0$ and $C_O(E) \to 1$, respectively, and we retrieve Eqs. (3) and (4).

Since the $N \times N$ matrix $\mathbf{Y}(E)$ is essentially a constant across threshold, the multichannel threshold behavior in Eq. (5) is simply determined by the threshold properties of the individual channels that participate in the close coupling. Each channel $|i\rangle$, with a given asymptotic threshold energy E_i^∞, is characterized by four channel parameters ξ_i, ν_i, λ_i, and C_i which are functions of the asymptotic kinetic energy $\varepsilon_i = E - E_i^\infty$. These parameters can be calculated separately, and economically, over any interesting mesh of total energies, while $\mathbf{Y}(E)$ need only be determined at one or two widely separated energies, and $\mathbf{S}_{OO}(E)$ can easily be constructed. We have written numerical codes which can calculate the four required QDT parameters for any given reference potential we may choose to associate with a given channel. This will be discussed in Sec. III, with the detailed algorithms presented in Appendix A. Furthermore, we have developed CC scattering codes, using the Milne function approach [10–12], which yield $\mathbf{Y}(E)$. The numerical procedures are found in Appendix B.

An example of the analytical behavior of $\mathbf{Y}(E)$ is given in Fig. 1, where the various matrix elements $\mathbf{Y}$ for a six-channel CC calculation are seen to be invariant across the three thresholds occurring at $E/E_{HF} = 0$, 1, and 2. These results will be discussed in greater detail in the next few sections, but this figure does illustrate the salient feature we are driving towards. Given $\mathbf{Y}$, the detailed resonant and threshold structure exhibited by the squared transition matrix elements $|\mathbf{T}_{OO}|^2 = |\mathbf{1} - \mathbf{S}_{OO}|^2$ in Fig. 1 is analytically given by the properties we extract from the reference functions f_i and g_i.

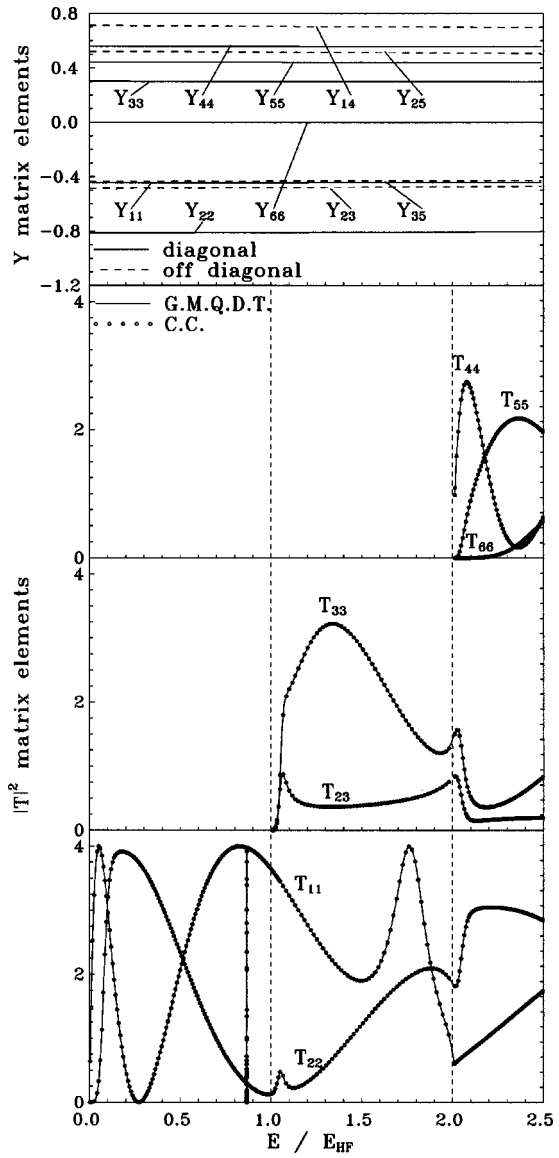

FIG. 1. Comparison of six-channel ($F=0$, $p=+1$) GMQDT and CC calculations. Energy-ordered channels are labeled from 1 to 6. The top panel demonstrates the negligible energy variation of the adiabatic $\mathbf{Y}(E)$ matrix computed at $R_o=35$ a.u. Only off-diagonal $|T_{ij}|^2$ elements involving exchange interaction are plotted. Three lower panels show the energy variation of $|T_{ij}|^2$ associated with the three hyperfine thresholds (marked by vertical lines: $E_{\rm HF}=0.0591\,{\rm cm}^{-1}=85.0\,{\rm mK}$). The solid curve shows GMQDT results in excellent agreement with exact CC results (full circles), with $\mathbf{Y}(E)$ linearly interpolated between $E_{\rm min}=-0.2\,{\rm cm}^{-1}$ and $E_{\rm max}=+0.2\,{\rm cm}^{-1}$. The GMQDT parameters C^{-1}, tan(λ), and phase shift ξ are evaluated at $R=400$ a.u., the same distance used to obtain the CC results.

The figure also demonstrates the exact agreement that is achieved between the numerical CC results (circles) and the analytic GMQDT results (curve).

Mies and Julienne [9] already pointed out the important role played by $\tan\lambda$ and C^{-1} in understanding threshold laws. Obviously they measure the validity of the WKB approximation, and by implication define the energy range of the associated threshold laws. The expected threshold behavior of the four QDT parameters are summarized in Table II in Sec. III. Of utmost importance in this paper is the fact that, as $\varepsilon_i\rightarrow 0$, the parameter $C_i(E)^{-1}$ for the closing channel $|i\rangle$ vanishes as $k_i^{l_i+1/2}$ where l_i is the partial wave quantum number and $k=\sqrt{2\mu\varepsilon_i/\hbar^2}$ is the asymptotic wave number defined by the colliding atoms with reduced mass μ. This threshold behavior appears in the matrix element $\bar{R}_{i,j}=C_i^{-1}\{\cdots\}C_j^{-1}$ in Eq. (1.6), and is the origin of the so-called Wigner threshold laws that we associate with the off-diagonal elements $S_{i,j}$ in Eq. (1.5). We will see many examples of this expected threshold behavior. We also note that for $l>0$, $C^{-1}(E)$ is extremely sensitive to tunneling through the rotational barriers, and gives a powerful means of isolating the effects of shape resonances in a multichannel problem. Close to threshold an interesting ''multichannel'' shape resonance effect is introduced by the energy variation of $\tan\lambda_O$ that appears in the denominator of Eq. (6). In addition, the behavior of $C^{-1}(E)$ for $l=0$ at threshold is directly related to what have been called ''zero-energy'' resonances [13]. In view of space limitations most of this shape resonance phenomena will be demonstrated in a subsequent paper devoted to resonance threshold effects.

An implicit assumption in deriving the GMQDT expression (1.5) is that the couplings which contribute to the matrix $\mathbf{Y}$ are achieved at short range, at distances well before the reference channel parameters in Table II acquire their threshold behavior. Very long-range potential terms proportional to α^2R^{-3} play an important role in determining the spin depolarization cross sections in Eq. (1). The very long-range nature of these terms have a profound effect on the threshold laws and perturbative corrections must be applied to some of the MQDT matrix elements in Eq. (1.5). If we designate the scattering matrix elements generated by the short-range $\mathbf{Y}$ matrix in Eq. (1.5) as $\mathbf{S}_{OO}(\mathbf{Y})$, we can use the distorted-wave approximation (DWA) [14] to apply a perturbative long-range correction to these elements,

$$S_{i,j}=S_{i,j}(\mathbf{Y})+S_{i,j}^{\rm DWA}, \tag{1.7}$$

$$S_{i,j}^{\rm DWA}=-2\pi i\left\langle \varepsilon_i\left|\frac{C_{i,j}}{R^3}\right|\varepsilon_j\right\rangle, \tag{1.8}$$

where the energy-normalized continuum states $|\varepsilon_i\rangle$ and $|\varepsilon_j\rangle$ are defined by the reference potentials. This can be evaluated numerically and has been found to yield excellent results. This and several other aspects of the long-range interactions are discussed in detail in Sec. IV. A summary and conclusions are presented in Sec. V.

II. CLOSE-COUPLED DESCRIPTION OF HYPERFINE TRANSITIONS

In a field-free collision between Na atoms in Eq. (1.1), both the total angular momentum $\mathbf{F}=\mathbf{f}_a+\mathbf{f}_b+\mathbf{l}=\mathbf{f}+\mathbf{l}$ and the total parity $p=\pm 1$ are constants of motion and the collisional loss rate constants are derived from the appropriate sums involving the scattering matrices $\mathbf{S}_{OO}(\mathbf{F},p,E)$. These are calculated from standard CC codes for a given $\mathbf{F}$, p, and

TABLE I. $F=0$, parity $+1$ (a) and $F=1$, parity -1 (b) channel states. *Only channels with *identical* (l,f) are strongly coupled by the short-range exchange interaction in Eq. (2.7).

(a)

Channel	l	f	f_a	f_b	E^∞(mK)
1*	0	0	1	1	0.0
2	2	2	1	1	0.0
3	2	2	1	2	85.024
4*	0	0	2	2	170.048
5	2	2	2	2	170.048
6	4	4	2	2	170.048

(b)

Channel	l	f	f_a	f_b	E^∞ (mK)
1*	1	1	1	1	0.0
2*	1	1	1	2	85.024
3	1	2	1	2	85.024
4	3	2	1	2	85.024
5	3	3	1	2	85.024
6*	1	1	2	2	170.048
7	3	3	2	2	170.048

E, using the usual channel state basis $|F,M,p;l,f,f_a,f_b\rangle$ [4],

$$\Psi_i^+(F,M,p,E,R)=\sum_{j=l,f,f_a,f_b}|F,M,p;j\rangle F_{j,i}(E,R)/R, \tag{2.1}$$

which describes the asymptotic properties of the separated atoms, where l is the nuclear angular momentum (partial wave quantum number), and f represents the magnitude of the channel angular momentum $\mathbf{f}=\mathbf{f}_a+\mathbf{f}_b$. The channel states are appropriately symmetrized with respect to interchange of the atoms associated with the total atomic angular momenta $\mathbf{f}_a$ and $\mathbf{f}_b$, respectively. As F increases, up to 20 channels can contribute to $\mathbf{S}_{OO}(\mathbf{F},p,E)$. However, for $F=0$ and $p=+1$ only the six-channels list in Table I(a) contribute to the scattering, and most of our examples, such as those given in Fig. 1, will involve this simple case. This one set exhibits almost all the interesting effects we can project from GMQDT, with the exception of the frame transformation effects associated with degenerate channel states. These effects contribute to, and will be illustrated with, the seven channel $F=1$, $p=-1$ case listed in Table I(b).

The complete physics of the scattering problem is already dictated by the interaction matrix $W_{i,j}(R)$ that is used in solving the close-coupled equations. We presuppose that the finite set of molecular channel states $|j\rangle$ $(j=1,N)$ that has been included in the CC expansion of the total continuum wave function (2.1) is sufficiently complete to span the space of all coordinates (with the obvious exclusion of the radial interatomic coordinate R), or at least complete enough to describe all inelastic processes of importance at the prescribed total energy E. The $N\times N$ matrix of radial functions $\mathbf{F}(E,R)$ are obtained from a numerical solution of the following close-coupled equations [20],

$$\frac{\partial^2\mathbf{F}}{\partial R^2}+\left(\frac{2\mu}{\hbar^2}\right)[E-\mathbf{W}(R)]\mathbf{F}(R)=0, \tag{2.2}$$

where $\mu=m_Am_B/(m_A+m_B)$ is the reduced mass associated with the collision of $A+B$. The interaction matrix $\mathbf{W}(R)$ becomes asymptotically diagonal, and defines the internal energy E_i^∞ associated with each channel state $|i\rangle$ introduced in the expansion

$$W_{j,i}(R)\underset{R\to\infty}{\sim}[E_i^\infty+l(l+1)\hbar^2/2\mu R^2]\delta_{j,i}+O(R^{-s}), \tag{2.3}$$

where $s\geqslant 3$. To be perfectly general we could include a Coulomb potential, with $s=1$, but this merely introduces needless complications which we do not require, and has already been elegantly treated in the vast body of MQDT literature [15] (see Ref. [16] for a collection of the literature).

If we impose N well-behaved boundary conditions on $\mathbf{F}(E,R)\to 0$ as $R\to 0$, we can obtain N independent solutions which satisfy Eq. (2.2). Given the asymptotic kinetic energy $\varepsilon_i=E-E_i^\infty$, and the associated asymptotic wave number $k_i(E)=\sqrt{(2\mu\varepsilon_i/\hbar^2)}$ for each channel, the set of N channels are seen to include N_O open channels, $\varepsilon_i>0$, with k_i real and positive, and N_C closed channels, $\varepsilon_i<0$, with imaginary $k_i=e^{i\pi/2}|k_i|$. Thus we can block the matrix $\mathbf{F}$ as

$$\mathbf{F}=\begin{bmatrix}\mathbf{F}_{OO} & \mathbf{F}_{OC}\\ \mathbf{F}_{CO} & \mathbf{F}_{CC}\end{bmatrix}. \tag{2.4}$$

If we impose well-behaved asymptotic boundary conditions $\mathbf{F}_{CO}\to 0$ on the closed-channel components of the first N_O set of column solutions vectors we obtain a total of N_O well-behaved solutions which are normalizable and correspond to physically meaningful continuum *wave functions*. The remaining set of N_C solution vectors all contain asymptotically diverging elements in $\mathbf{F}_{CC}$, and must be rejected as mathematically correct, but physically meaningless solutions. These conditions imply that we expect $\mathbf{F}_{OO}$ to asymptotically yield an accurate $(N_O\times N_O)$ reactance matrix $\mathbf{K}_{OO}(E)$, i.e.,

$$F_{OO}(E,R)\underset{R\to\infty}{\sim}[J_O(\varepsilon,R)+N_O(\varepsilon,R)\mathbf{K}_{OO}(E)]\mathbf{A}_{OO}^+, \tag{2.5}$$

where $J_i\to k_i^{-1/2}\sin(k_iR-\pi l/2)$ and $N_i\to k_i^{-1/2}\cos(k_iR-\pi l/2)$ conform to the usual spherical Bessel functions associated with the nuclear angular momentum l for the open channels $i=1$, N_O in Eq. (2.3) (see Appendix C of Ref. [17]). Note that $[J_O(\varepsilon,R)+N_O(\varepsilon,R)\mathbf{K}_{OO}(E)]$ represents the asymptotic form for a particular set of N_O solutions to Eq. (2.2). We can always chose any linear combinations of these to define a variety of equally exact well-behaved solutions. The matrix $\mathbf{A}_{OO}^+(E)$ in Eq. (2.5) is used to impose the usual incoming plane-wave scattering boundary conditions on the wave functions Ψ_i^+ in Eq. (2.1). Given $\mathbf{K}_{OO}$ we choose $\mathbf{A}_{OO}^+(E)=[1-i\mathbf{K}_{OO}(E)]^{-1}$, and obtain the associated scattering matrix $\mathbf{S}_{OO}(E)$ which defines the dynamic properties of the system:

$$\mathbf{S}_{OO}(E)=[1+i\mathbf{K}_{OO}(E)][1-i\mathbf{K}_{OO}(E)]^{-1}. \quad (2.6)$$

Making the reasonable assumption that the molecular hyperfine Hamiltonian can be adequately represented by a unitary frame transformation of the asymptotic atomic hyperfine Hamiltonians, the accuracy of the interaction matrix $W_{j,i}$ is basically limited by the accuracy of the molecular interactions we incorporate in our CC scattering codes. To perform the dynamic calculations, we require four accurate molecular potentials $V_{S,\Omega}(R)$: one defined by the ground $X\ ^1\Sigma_g^+$ state with $S=0$ and with molecule-fixed spin projection $\Omega=0$; and three defined by the lowest $a\ ^3\Sigma_u^+$ state with $S=1$ and spin projections $\Omega=0,\pm1$. These potentials take the following asymptotic forms [4,18]:

$$V_{0,0}(R)\sim -C_{\rm exc}e^{-aR}+(C_6R^{-6}+C_8R^{-8}+C_{10}R^{-10}), \quad (2.7a)$$

$$V_{1,0}(R)\sim +C_{\rm exc}e^{-aR}+(C_6R^{-6}+C_8R^{-8}+C_{10}R^{-10}) + \alpha^2R^{-3}+V^{SO}_{\Omega=0}(R), \quad (2.7b)$$

$$V_{1,\pm1}(R)\sim +C_{\rm exc}e^{-aR}+(C_6R^{-6}+C_8R^{-8}+C_{10}R^{-10}) - 1/2\alpha^2R^{-3}+V^{SO}_{\Omega=\pm1}(R). \quad (2.7c)$$

The knowledge of these potentials is adequate to completely describe the ultracold collision dynamics of all the alkali atoms that have been studied to date. The terms proportional to α^2R^{-3} in Eqs. (2.7b) and (2.7c) are the so-called relativistic spin-spin (SS) or dipole-dipole interactions [19] which are second order in the fine-structure constant $\alpha\approx\frac{1}{137}$. The role of these terms in inducing spin depolarization has been elegantly treated in a series of papers by the Verhaar group [3]. The short-range second-order spin-orbit (SO) terms play a similar role, and in fact dominate over the SS terms, for the heavier alkalis [4,5], but are negligible for Na. As discussed above, the very long-range nature of the SS terms has a profound effect on the threshold laws, and perturbative corrections, given by Eqs. (1.7) and (1.8), must be applied to certain of the GMQDT matrix elements in Eq. (1.5). This and several other aspects of the long-range interactions are discussed in detail in Sec. IV C.

Two colliding ground-state alkali-metal atoms in (ns) orbitals, have, to good order, zero total electronic *orbital* angular momentum $\mathbf{L}=(\mathbf{L}_a+\mathbf{L}_b)\approx\mathbf{0}$. As a consequence, in the absence of the long-range SS or short-range SO interactions, the molecular Hamiltonian implies that l and f are good quantum numbers. The physical reason is that for $\mathbf{L}=\mathbf{0}$ there are no electrostatic interactions that cause a locking of the electron-spin angular momentum of the system to the internuclear axis. Ultimately, the weak SS and SO interactions cause the total electronic spin $\mathbf{S}=(\mathbf{s}_a+\mathbf{s}_b)$ to couple to the axis, and lead to small energetic splittings between Ω projections represented in Eq. (2.7). If we ignore these latter interactions the Ω projections are perfectly degenerate, and we can easily transform the asymptotic channel states $|F,M,p;l,f,f_a,f_b\rangle$ into a basis defined by the total electron-spin angular momentum S ($\mathbf{S}=\mathbf{s}_a+\mathbf{s}_b$) and the total nuclear spin I ($\mathbf{I}=\mathbf{i}_a+\mathbf{i}_b$), where $\mathbf{s}_a$ and $\mathbf{s}_b$ are the atomic electron-spin angular momenta, and $\mathbf{i}_a$ and $\mathbf{i}_b$ are the nuclear-spin angular momenta (for ^{23}Na, $s_a=s_b=\frac{1}{2}$ and $i_a=i_b=\frac{3}{2}$),

$$|F,M,p;l,f,S,I\rangle \propto\sum_{f_af_b}\sqrt{(2S+1)(2I+1)(2f_a+1)(2f_b+1)} \times\begin{Bmatrix} s_a & i_a & f_a\\ s_b & i_b & f_b\\ S & I & f\end{Bmatrix}|F,M,p;l,f,f_a,f_b\rangle. \quad (2.8)$$

In this representation [4] two adiabatic Born-Oppenheimer potentials, uniquely identified by the quantum numbers $S=0$ (from $X\ ^1\Sigma_g^+$) and $S=1$ (from $a\ ^3\Sigma_u^+$), appear on the diagonal of the Hamiltonian matrix. The hyperfine interactions can introduce a simultaneous change in I and S. However, these couplings are constrained to subblocks which insure that $\mathbf{f}=\mathbf{I}+\mathbf{S}$ is conserved, and we find both f and l remain perfectly good quantum numbers at all distances. Of course, at small distances, where the exchange splitting between the molecular potentials is large compared to the hyperfine splittings, even this coupling is negligible. However, as we shall see, at distances of the order $R\approx(20-40)a_O$, the hyperfine interaction becomes important and the $I\leftrightarrow S$ coupling drives the system back into the asymptotically diagonal basis of channel states $|F,M,p;l,f,f_a,f_b\rangle$.

III. SUMMARY OF MQDT THEORY UTILIZING MILNE FUNCTIONS

The $N_O\times N_O$ matrix of radial functions $\mathbf{F}_{OO}(E,R)$ in Eq. (2.5) is obtained from a numerical solution of the CC equations, and yields the associated scattering matrix $\mathbf{S}_{OO}(E)$ in Eq. (2.6), which fully defines the dynamic properties of the system. The goal of GMQDT is to represent these *same* exact solutions to the *same* set of close-coupled scattering equations in a form that is an analytic function of the total energy E, especially as we cross thresholds. The final result achieved is given in Eq. (1.5).

We begin by *choosing* a set of reference potentials $V_j(R)$ that we will associate with each of the $j=1,N$ channel states $|j\rangle$ that have been included in the close-coupled expansion of the total continuum wave function. As summarized in Table III of Appendix A, each reference potential defines a pair of reference radial functions $f_i(\varepsilon_i,R)$ and $g_i(\varepsilon_i,R)$ *analytic* in the asymptotic kinetic energy $\varepsilon_i=E-V_i(\infty)$ prescribed by E. This allows us to represent the exact close-coupled solutions to Eq. (2.2) in the following matrix form [20].

$$\mathbf{F}(E,R)=[f(\varepsilon,R)+g(\varepsilon,R)\mathbf{Y}(E,R)]\mathbf{A}(E,R). \quad (3.1)$$

Assuming that each reference potential has been chosen to have the exact asymptotic behavior prescribed by the exact interaction matrix $\mathbf{W}$ in Eq. (2.3), the matrices $\mathbf{Y}(E,R)\rightarrow\mathbf{Y}(E)$ and $\mathbf{A}(E,R)\rightarrow\mathbf{A}(E)$ will approach constants at some *finite* distance, and the asymptotic solutions approach

$$\mathbf{F}(E,R)\underset{R\rightarrow\infty}{\sim}[f(\varepsilon,R)+g(\varepsilon,R)\mathbf{Y}(E)]\mathbf{A}(E). \quad (3.2)$$

If we choose a reasonable set of reference potentials $V(R)=\{Vi(R)\delta_{i',i}\}$ to define the associated sets of independent reference functions $f(\varepsilon,R)=\{f_i(\varepsilon_i,R)\delta_{i',i}\}$ and $g(\varepsilon,R)=\{g_i(\varepsilon_i,R)\delta_{i',i}\}$ which are properly analytic in E, we can insure that the matrix $\mathbf{Y}(E)$ is also analytic, and can be safely extrapolated across thresholds as various channels open and close. The dynamics prescribed by the scattering matrix in Eq. (1.5) is completely determined by the real symmetric analytic matrix $\mathbf{Y}(E)$, and of course the asymptotic properties of the analytic reference functions. An example of this behavior has already been given in Fig. 1, where the various matrix elements $\mathbf{Y}$ for this six-channel CC calculation are seen to be essentially constant across three thresholds. Given $\mathbf{Y}$, the detailed resonant and threshold structure exhibited in Fig. 1 is given by the properties we extract from the reference functions f and g. Note that the nonanalytic matrix $\mathbf{A}(E)$ remains at our disposal, and can be used to asymptotically normalize the radial solutions $\mathbf{F}(E,R)$ to conform to Eqs. (2.4)–(2.6). An explicit evaluation of $\mathbf{A}(E)$ is only required to describe *half-collision* processes such as photodissociation [26], where the short-range properties of the energy-normalized continuum wave functions are required.

The relationship between GMQDT and conventional scattering theory becomes quite apparent when comparing Eqs. (3.2) and (2.5). The usual ansatz in CC scattering theory is to asymptotically match the exact or numerically derived scattering wave function $\mathbf{F}_{OO}$ in Eq. (2.5) directly with the well-defined spherical Bessel functions $J_i(\varepsilon_i,R)$ and $N(\varepsilon_i,R)$. This yields, by definition, the reactance matrix $\mathbf{K}_{OO}$ and the scattering matrix $\mathbf{S}_{OO}$ that are needed to calculate observable cross sections. This procedure relies on Eq. (2.3), and recognizes that each *open* channel is associated, at least asymptotically, with some well-defined partial wave with an angular momentum quantum number l and a concomitant centrifugal potential proportional to $l(l+1)/R^2$. Since the Bessel functions represent exact solutions to the centrifugal portion of Eq. (2.3), we merely need integrate $\mathbf{F}_{OO}(E,R)$ out to some very large but finite distance where all residual interaction matrix elements become small compared to $1/R^2$, and where $\mathbf{F}_{CO}$ can be made to exponentially vanish. In this case the resultant numerical multichannel $\mathbf{K}_{OO}(E)$ is extremely energy dependent, and implicitly incorporates all the resonant and threshold behavior inherent in the dynamics involving both open and closed channels. As already implied in Eqs. (1.3)–(1.6), we will find that the bulk of this energy dependence is introduced by the higher-order terms associated with the *diagonal* elements in Eq. (2.3).

In the GMQDT expression (3.2) we go one step further, and substitute a different but equally valid independent pair of *analytic* reference functions $f(\varepsilon,R)$ and $g(\varepsilon,R)$ with which to fit the exact solution vectors. These are defined by whatever particular set of diagonal reference potentials $V=\{V_i\delta_{j,i}\}$ we have decided will most effectively summarize the dynamics. Certainly we expect V_i to incorporate the leading asymptotic c_iR^{-s} dependence implied in Eq. (2.3), which means we can terminate the integration of $\mathbf{F}(E,R)$ at a much smaller distance R where the exact $f(\varepsilon,R)$ and $g(\varepsilon,R)$ basis now replaces the Bessel functions. Furthermore, given the analytic properties of the reference functions we can now evaluate the closed channel components $\mathbf{F}_{OC}(E,R)$ at small R, and explicitly enumerate the resonance contribution as in Eq. (1.4).

Although we have employed the notation and analysis of Refs. [8], [9], several other comparable studies have been devoted to a generalization of QDT to non-Coulomb potentials [10–12,21], and more explicitly to long-range R^{-s} reference potentials [22–24]. Recently a very ingenious set of *standardized long-range* references functions were defined by Burke, Greene, and Bohn [12], which have the virtue of offering a compact representation of multichannel cold-atom dynamics which is easily converted to observables. However the present analysis relies on using the Milne solutions in Appendix A to generate exact reference functions for any prescribed $V(R)$, and is committed to choosing $f(\varepsilon,R)$ to be well behaved as $R\rightarrow 0$. One very useful feature of this choice is that $\mathbf{Y}(E,R)$, which begins at zero at $R=0$, can be followed as a function of R, and allows us to pinpoint exactly where and between what channels the close coupling is occurring. This feature is demonstrated in Sec. IV. Furthermore the resultant $\mathbf{Y}(E)$ should be less energy dependent since $f(\varepsilon,R)$, and its associated phase shift, already incorporates the energy variation of the short-range potential. Finally, an important virtue is that $f(\varepsilon,R)$ can often be used to obtain reliable perturbative estimates of the $\mathbf{Y}(E)$ matrix elements [25,26], or explicitly used in DWA expressions such as Eq. (1.8).

It cannot be emphasised too strongly that the quality of the calculations is independent of our choice of reference potential $V(R)$. In principle, the wisdom of our choice of $V(R)$ is irrelevant since the dynamics has already been prescribed for us by whatever interaction matrix $\mathbf{W}(R)$ has been used to solve the coupled equations (2.2) for $\mathbf{F}$. Again this feature is shown in Fig. 1, where close-coupled and GMQDT calculations are seen to give identical results.

Two rather obvious choices of reference potentials can be made. The first we call the diabatic basis where we take $V_j(R)=W_{j,j}(R)$. Alternatively we often use the adiabatic basis [8–10,17] obtained by diagonalizing the exact close-coupled interaction matrix, $\mathbf{W}=\mathbf{M}\mathbf{V}^O\tilde{\mathbf{M}}$. Of course, since in our scheme we obtain $\mathbf{Y}(E)$ from an exact solution of the coupled equations, using the exact interaction matrix $\mathbf{W}$, it does not really matter which basis we use—the combination of $\mathbf{Y}(E)$ and the associated channel parameters together are guaranteed to always give the exact $\mathbf{S}_{OO}(E)$. However, two considerations may help in choosing the basis. If one wants to explore close coupling over an extensive range of energies, then we would like a basis which yields the most slowly varying $\mathbf{Y}(E)$. If one wishes to develop perturbative approximations [25,26], then the basis with the smallest $\mathbf{Y}(E)$ elements would be preferable. Of the two, we generally find the adiabatic basis to be the most useful. However, in the present case, because of the marked differences between the strongly coupled short-range exchange interaction and the weakly coupled long-range SS interaction, we have found it most instructive to use a mixed basis.

We choose to *separately* diagonalize the individual blocks of channels with equivalent l, and use these diagonalized

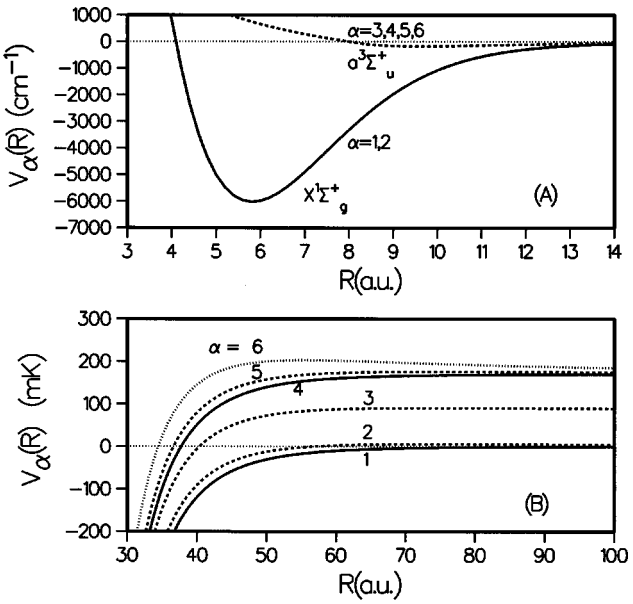

FIG. 2. (A) Reference potentials for the $F=0$, $p=+1$ channel states $\alpha=1-6$. Subblocks of channels with a given nuclear angular momenta l are diagonalized separately. At short distances the $l=0$ channel $\alpha=1$ and the $l=2$ channel $\alpha=2$ adiabatically correlate with the $X\ ^1\Sigma_g^+$ state. All the remaining channels adiabatically correlate with the $a\ ^3\Sigma_u^+$ state. (B) Asymptotic correlations of the $F=0$, $p=+1$ solid ($l=0$), dashed ($l=2$), and dotted ($l=4$) channels. See Table I for a description of asymptotic properties. $E_{HF}=85.024$ mK.

elements as our reference potentials. In this way l persists in remaining a well-defined quantum number throughout the analysis, and the coupling between different l blocks remains diabatic and amenable to perturbation theory. For example, the three $l=2$ channels in the $F=0$ case in Table I(a) are strongly coupled by the exchange interaction, and when diagonalized yields the reference potentials $\alpha=2$, 3, and 5 in Fig. 2, where, at small R, and out to where the exchange interaction term $C_{\rm exc}$ in Eq. (2.7) remains dominant, $\alpha=2$ correlates with $X\ ^1\Sigma_g^+$, and $\alpha=3$ and 5 correlate with $a\ ^3\Sigma_u^+$. As seen in Fig. 2, the diagonalization of the two $l=0$ channel interactions yield the reference potential $\alpha=1$ which correlates with $X\ ^1\Sigma_g^+$ and the $\alpha=4$ potential which correlates with $a\ ^3\Sigma_u^+$. The single $l=4$ channel, designated $\alpha=6$, corresponds to a pure triplet state, and only couples to the other channels by SS coupling. The basis we have chosen for $F=1$ consists of two separate adiabatic blocks for $l=1$ and 3, each of which contains a single channel which correlates with $X\ ^1\Sigma_g^+$, with the remainder correlating with $a\ ^3\Sigma_u^+$.

Returning to Eq. (3.2), we block the $N\times N$ matrix of solutions vectors $\mathbf{F}$ into open and closed subsets, designated by sub O and sub C indices [20];

$$\mathbf{F}=\begin{bmatrix} f_O+g_O\mathbf{Y}_{OO} & g_O\mathbf{Y}_{OC} \\ g_C\mathbf{Y}_{CO} & f_C+g_C\mathbf{Y}_{CC}\end{bmatrix}\begin{bmatrix}\mathbf{A}_{OO} & \mathbf{A}_{OC} \\ \mathbf{A}_{CO} & \mathbf{A}_{CC}\end{bmatrix} \tag{3.3}$$

The single index O or C on the reference functions f and g are meant to indicate diagonal matrices which contribute to the blocks OO or CC. Since the $g_C\mathbf{Y}_{CO}$ component in the first N_O columns of solution vectors is always exponentially rising, none of the solutions are physically meaningful.

Although only two independent reference solutions can exist for each channel, the pair of *analytic* functions $f(\varepsilon,R)$ and $g(\varepsilon,R)$ can be used to define a variety of special solutions, as in Table III of Appendix A, which satisfy various interesting boundary conditions. *All* these solutions are uniquely specified by the single amplitude $\alpha(\varepsilon,R)$ and the associated phase $\beta(\varepsilon,R)$ which we obtain from solution of the Milne equation with the analytic WKB-like boundary conditions imposed on $\alpha(\varepsilon,R_e)$ and $\alpha'(\varepsilon,R_e)$ at the equilibrium distance R_e associated with the reference potential.

As discussed in Appendix A, for closed channels both $f\rightarrow\sin\nu Ae^{+|k|R}+\cos\nu Be^{-|k|R}$ and $g\rightarrow\cos\nu Ae^{+|k|R}-\sin\nu Be^{-|k|R}$ are exponentially divergent as $R\rightarrow\infty$. It is one of the major chores of GMQDT to find the particular linear combination of channel reference functions which decays asymptotically whenever a channel is closed. This is designated by the function $\phi(\varepsilon,R)$ in Table III, i.e., for $\varepsilon<0$, and $R\rightarrow\infty$:

$$\phi(\varepsilon,R)=[f(\varepsilon,R)\cos\nu(\varepsilon)-g(\varepsilon,R)\sin\nu(\varepsilon)]\rightarrow Be^{-|k|R}. \tag{3.4}$$

This combination is defined by what we often call the *bound-state* phase $\nu(\varepsilon)$ in Eq. (A5), which is analytic throughout $\varepsilon<0$, in contrast to the scattering phase shift $\xi(\varepsilon)$ which is analytic throughout $\varepsilon>0$, and might well be called the *continuum-state* phase.

Choosing $\mathbf{A}_{OO}=\mathbf{B}_{OO}$ and $\mathbf{A}_{CO}=-(\tan\nu_C+\mathbf{Y}_{CC})^{-1}\mathbf{Y}_{CO}\mathbf{B}_{OO}$ in Eq. (3.3) we obtain a new set of N_O solutions,

$$\mathbf{F}_{OO}=(f_O+g_O\overline{\mathbf{Y}}_{OO})\mathbf{B}_{OO} \tag{3.5a}$$

$$\mathbf{F}_{CO}=\frac{-\phi_C}{\cos\nu_C}(\tan\nu_C+\mathbf{Y}_{CC})^{-1}\mathbf{Y}_{CO}\mathbf{B}_{OO}, \tag{3.5b}$$

where $\mathbf{F}_{CO}$ is well behaved and vanishes asymptotically as required in Eq. (2.4). Since we can never choose any $\mathbf{A}_{OC}$ and $\mathbf{A}_{CC}$ coefficients which will avoid the divergences in the closed channels, we conclude, as in Eq. (2.4), that we must reject the remaining set of N_c solution vectors as physically meaningless.

The open-channel block of radial solution vectors $f_O+g_O\overline{\mathbf{Y}}_{OO}$ in Eq. (3.5a) now involves the transformed $\overline{\mathbf{Y}}_{OO}$ matrix defined in Eq. (1.4), which is seen to embody the resonant coupling to the closed channels through the resonance sensitive denominator $(\tan\nu_C+\mathbf{Y}_{CC})$. In previous studies [8–11] we have very carefully considered the effects of closing various subsets of channels. This gives rise to a resonance structure that manifests itself as predissociation in atom-atom scattering processes, and as autoionization in electron-ion scattering. This effect, particularly its threshold behavior, will be demonstrated in detail in a subsequent paper.

To finally extract the scattering matrix we need to know the asymptotic properties of the open-channel block $f_O + g_O\overline{\mathbf{Y}}_{OO}$ in Eq. (3.5a), which requires knowing the asymptotic properties of the open, channel reference functions f_O and g_O. As seen in Table III, the pair of analytic functions $f(\varepsilon,R)$ and $g(\varepsilon,R)$ are expressed in terms of a second pair of independent functions s and c:

$$f(\varepsilon,R)=\alpha\sin\beta=Cs(\varepsilon,R), \tag{3.6a}$$

$$g(\varepsilon,R)=\alpha\cos\beta=C^{-1}[c(\varepsilon,R)-(\tan\lambda)C^2s(\varepsilon,R)], \tag{3.6b}$$

which have the well-defined asymptotic boundary conditions that we require,

$$s(\varepsilon,R)\underset{R\to\infty}{\sim}(\cos\xi)J(\varepsilon,R)+(\sin\xi)N(\varepsilon,R)\to k^{1/2}\sin(kR-\pi l/2+\xi), \tag{3.7a}$$

$$c(\varepsilon,R)\underset{R\to\infty}{\sim}(-\sin\xi)J(\varepsilon,R)+(\cos\xi)N(\varepsilon,R)\to k^{1/2}\cos(kR-\pi l/2+\xi), \tag{3.7b}$$

where $J(\varepsilon,R)$ and $N(\varepsilon,R)$ conform to the spherical Bessel functions in Eq. (2.5). Note that $s(\varepsilon,R)$, which is well behaved at $R=0$, is the usual energy-normalizable continuum wave function defined by the prescribed reference potential at any energy above threshold $\varepsilon>0$. To make Eq. (3.5) consistent with Eq. (2.5), we must set $\mathbf{B}_{OO}=[1_O-(\tan\lambda_O)\overline{\mathbf{Y}}_{OO}]^{-1}C_O^{-1}[1_O-i\overline{\mathbf{R}}_{OO}]^{-1}e^{i\xi_O}$. Multiplying $(f_O+g_O\overline{\mathbf{Y}}_{OO})$ from the right by $[1_O-(\tan\lambda_O)\overline{\mathbf{Y}}_{OO}]^{-1}C_O^{-1}$ we obtain $s_O+c_O\overline{\mathbf{R}}_{OO}$, with $\overline{\mathbf{R}}_{OO}$ defined by Eq. (1.6). Further multiplication by $[1_O-i\overline{\mathbf{R}}_{OO}]^{-1}e^{i\xi_O}$ then leads to expression (1.5) for S_{OO}.

Well above threshold, as $C(E)\to1$ and $\tan\lambda(\varepsilon)\to0$, the asymptotic behavior of the analytic functions is exactly given by Eq. (3.7), and $\overline{\mathbf{R}}_{OO}\to\overline{\mathbf{Y}}_{OO}$. Viewed in reverse we see that the usual energy-normalizable continuum wave functions $s(\varepsilon,R)$ and $c(\varepsilon,R)$,

$$s(\varepsilon,R)=C^{-1}(\varepsilon)f(\varepsilon,R), \tag{3.8a}$$

$$c(\varepsilon,R)=C(\varepsilon)\{g(\varepsilon,R)+[\tan\lambda(\varepsilon)]f(\varepsilon,R)\}, \tag{3.8b}$$

only conform to the analytic reference functions at energies sufficiently removed from threshold, where $C(\varepsilon)\to1$ and $\tan\lambda(\varepsilon)\to0$. These conditions imply that the WKB approximation gives a valid description of the wave functions from $R=R_e$ where we set the boundary conditions on the analytic functions f and g, out to infinity where the boundary conditions for the s and c functions are obtained. However, as $\varepsilon\to0^+$, f and g begin to lose the asymptotic phase relationship implied by Eq. (3.7), and their asymptotic behavior requires the introduction of the two additional MCQDT parameters $C(\varepsilon)$ and $\tan\lambda(\varepsilon)$, which appear in Eq. (3.6) and markedly influence the threshold energy dependence of $\mathbf{S}_{OO}$.

TABLE II. Threshold laws for MQDT parameters for $V\sim R^{-s}$ reference potentials.

(1)	$\xi(\varepsilon)\underset{\varepsilon\to0^{\pm}}{\longrightarrow}(-A_l\lvert k\rvert)^{2l+1}$	$2l+1\leqslant(s-2)$ [a]
	$\xi(\varepsilon)\underset{\varepsilon\to0^{+}}{\longrightarrow}k^{s-2}$	$2l+1>(s-2)$
(2)	$1/C^2(\varepsilon)\underset{\varepsilon\to0^{\pm}}{\longrightarrow}(B_l\lvert k\rvert)^{2l+1}$	all l
(3)	$\tan\lambda(\varepsilon)\underset{\varepsilon\to0^{+}}{\longrightarrow}\tan\lambda(0)-O\left(\frac{1}{C^4(\varepsilon)}\right)$	
(4)	$\cot\nu(\varepsilon)\underset{\varepsilon\to0^{-}}{\longrightarrow}\cot\nu(0)+\frac{(-1)^l}{C^2(\varepsilon)}$	
(5)	$\tan\lambda(0)\tan\nu(0)=-1$	

[a]Except for $s=3$, $l=0$, which approaches $kln(k)$ [36,37].

The threshold laws obeyed by the four QDT parameters are summarized in Table II, and are a sensitive function of the asymptotic power dependence R^{-s} associated with the reference potential defined by Eq. (2.3). We see no necessity to present a very lengthy and tedious analysis based on the analytic properties of the spherical bessel functions that lead to Table II. Certainly the threshold behavior for the phase shift is well documented in the scattering literature. It is sufficient to note that the remaining threshold laws in Table II have been thoroughly and completely confirmed by numerical results obtained from the Milne analysis in Appendix A. We shall see examples with $s=6$ and 3. A detailed discussion of the analytic properties of various quantum defect parameters using Jost functions is given by Greene and coworkers [21] and Rau [27], but the parameters are defined somewhat differently than here, and the threshold behavior is not made as explicit as in Table II. The consequences of these various dependences are discussed and demonstrated in detail in Sec. IV.

IV. COMPARISON TO EXACT CLOSE-COUPLING RESULTS

A. Exchange and short-range coupling

At short range there is a strong coupling between certain channels which is associated with the exchange terms $C_{\rm exc}e^{-aR}$ in Eq. (2.7). This exchange coupling *always* conserves the channel quantum numbers (f,l), and occurs for example between channels 1 and 4, and between channels 2, 3, and 5 in Table I(a). This short-range behavior is nicely demonstrated in Fig. 3. $\mathbf{Y}(E,R)$ begins to deviate from zero in the vicinity of $R=18$ a.u., where the exchange splitting between the $X\ ^1\Sigma_g^+$ and $a\ ^3\Sigma_u^+$ state potentials ($V_{0,0}$ and $V_{1,\Omega}$) becomes comparable to the atomic hyperfine level splitting. For these particular channels $\mathbf{Y}(E,R)\to\mathbf{Y}(E)$ already approaches its asymptotic limit by about $R=35$ a.u., where the exchange splitting becomes completely negligible. As expected, only elements conforming to the constraint $(f,l)=$const have any significant magnitude. Note that the abrupt behavior of the adiabatic $\mathbf{Y}$ matrix elements in the vicinity of $R=23$ a.u. is simply due to a nearly diabatic curve

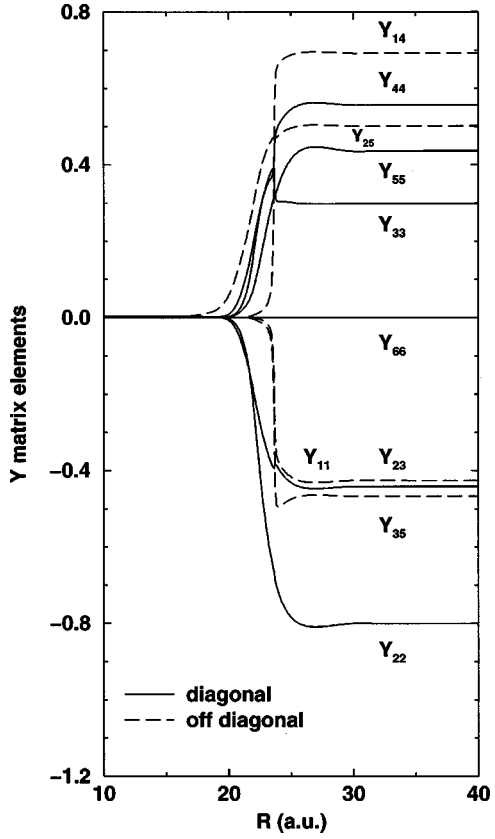

FIG. 3. R variation of the $\mathbf{Y}(E,R)$ matrix elements (six-channel case, $F=0$, even parity). Only the off-diagonal matrix elements induced by short-range exchange interactions are plotted. $\mathbf{Y}(E)$ has been evaluated at $E=0.2\ \mathrm{cm}^{-1}$, when all channels are open. In this example completely adiabatic reference potentials were used.

crossing of channel 4 with channels 2 and 3, which are coupled by the weak SS interaction. This behavior becomes even more apparent in Sec. IV B.

In Fig. 1 we demonstrated the perfect agreement that is obtained between the CC and adiabatic GMQDT results for the six-channel case. ($F=0$, $p=+1$). Note, however, that we have only presented the results for channels 1 and 4, and for channels 2, 3, and 5 which are strongly coupled by the short-range exchange interactions. In the top panel we can see that the energy variation of the adiabatic $\mathbf{Y}$ matrix is negligible throughout the region from the threshold for the $(f_a,f_b)=(1,1)$ channels at $E/E_{HF}=0$ to beyond the $(f_a,f_b)=(2,2)$ threshold at $E/E_{HF}=2$. $\mathbf{Y}(E)$ is computed at $R_O=35$ a.u., at which point exchange interactions become negligible. This result suggests that we can numerically evaluate $\mathbf{Y}(E)$ at two energies of our choice $E_{\min}$ and $E_{\max}$, and then use a linear interpolation of the $\mathbf{Y}(E)$ matrix for energies in between. The GMQDT calculations shown in Fig. 1 actually correspond to a $\mathbf{Y}$ matrix linearly interpolated between $E_{\min}=-0.2$ and $E_{\max}=+0.2\ \mathrm{cm}^{-1}$.

The log-log plot in Fig. 4 shows the exchange dominated inelastic transition matrix elements in the vicinity of the $(f_a,f_b)=(2,2)$ threshold. The diagonal elements are presented in Fig. 5. In this case we have used the mixed basis of reference potentials discussed in Sec. III. Again, the energy variation of the $\mathbf{Y}$ matrix is negligible, and we again obtain

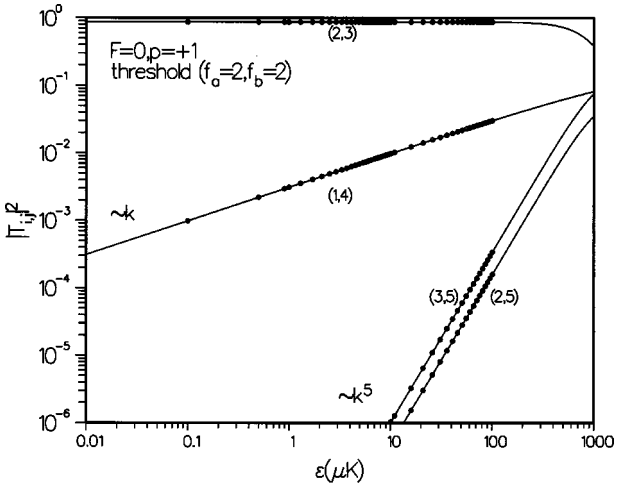

FIG. 4. Exchange-dominated *off-diagonal* $|T_{ij}|^2$ elements for the six-channel ($F=0$, $p=+1$) case in Table I(a). ε is measured relative to the $f_a=2$, $f_b=2$ threshold, where all channels are open. The analytic GMQDT results (circles) compare perfectly with the exact CC results (solid line). $|T_{14}|^2$ exhibits the k dependence expected for a closing $l=0$ channel, while $|T_{25}|^2$ and $|T_{35}|^2$ conform to the k^5 threshold law expected for a closing $l=2$ channel. CC T-matrix elements were evaluated at $R_{\max}>70\,000$ a.u.

perfect agreement between the CC and GMQDT results, confirming that our GMQDT results are not dependent on the choice of reference potentials.

Using Eq. (1.5) the transition matrix $\mathbf{T}_{OO}$ can be represented as

$$\mathbf{T}_{OO}=(1-\mathbf{S}_{OO})$$
$$=(1-e^{i2\xi_O})-2ie^{i\xi_O}\overline{\mathbf{R}}_{OO}(1-i\overline{\mathbf{R}}_{OO})^{-1}e^{i\xi_O}, \tag{4.1a}$$

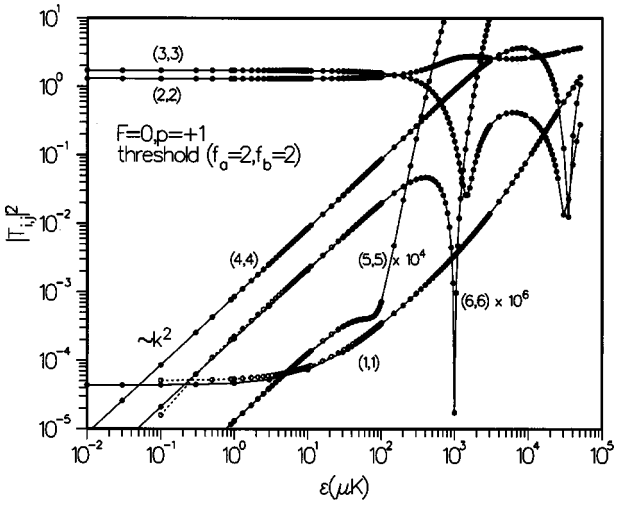

FIG. 5. Diagonal $|T_{ii}|^2$ elements for the six-channel ($F=0$, $p=+1$) case, same conditions as in Fig. 4. Dashed curves with open circles are the GMQDT results. Solid curves with solid dots are the CC results. Below $\varepsilon=10\ \mu$K the elements $|T_{44}|^2$, $|T_{55}|^2$, and $|T_{66}|^2$ show the k^2 expected for a long-range R^{-3} potential. At higher energies both elements $|T_{55}|^2$ and $|T_{66}|^2$ switch to a k^8 dependence associated with an R^{-6} potential.

which is equivalent to the following:

$$\mathbf{T}_{OO}=(1-e^{i2\xi_O})-2iC_O^{-1}e^{i\xi_O}\times[\overline{\mathbf{Y}}_{OO}^{-1}-(\tan\lambda_O+iC_O^{-2})]^{-1}C_O^{-1}e^{i\xi_O}. \quad (4.1b)$$

Because of the $C_i^{-1}(E)$ and $C_j^{-1}(E)$ parameters which bracket the element $\overline{R}_{i,j}(E)$ in Eq. (1.6), the threshold energy dependence of the *inelastic* $|T_{i,j}(E)|^2$ element, with $i\neq j$, as channel i approaches threshold, is determined by the energy variation of $C_i^{-2}(E)$. For those channels with $\varepsilon\gg 0$ we expect a WKB-like behavior which defines $C_i=1$. However, for closing channels this parameter has the limiting form $C^{-1}(\varepsilon)\rightarrow(B_l k)^{l+(1/2)}$ as $\varepsilon\rightarrow 0^+$, and yields the expected Wigner threshold law $|T_{i,j}|^2=|T_{j,i}|^2\propto k_i^{2l+1}$.

The element $|T_{14}|^2$ in Fig. 4 exhibits the prescribed k dependence for a closing $l=0$ channel, while the $|T_{25}|^2$ and $|T_{35}|^2$ elements show the expected k^5 dependence for closing $l=2$ channels. Actually, in cases involving shape resonances, as seen in the vicinity of the channel 3 threshold in Fig. 1, which involves an $l=2$ incident partial wave, there can also be a substantial *increase* in C_i^{-2}, indicating an enhanced tunneling of amplitude across the centrifugal barrier. This interesting behavior will be explored in more detail in a subsequent paper devoted to threshold resonance phenomena. However, even in this case, if we approach close enough to threshold, the predicted threshold laws will eventually prevail, and indeed we find that the $|T_{23}|^2$ matrix element ultimately approaches the expected k^5 dependence for a closing $l=2$ channel.

To understand the origin of the C^{-1} behavior and its influence on $\overline{\mathbf{R}}_{OO}$, recall that both $f(\varepsilon,R)$ and $s(\varepsilon,R)$ are well behaved at $R=0$, but the second boundary condition for $f(\varepsilon,R)$ has been set at $R=R_m$ to insure that this function is analytic across the threshold $\varepsilon=0$, while $s(\varepsilon,R)$ has been set at infinity to give the usual energy normalizable boundary condition, i.e., $\langle s(\varepsilon)|s(\varepsilon')\rangle=(\pi\hbar^2/2\mu)\delta(\varepsilon-\varepsilon')$. The initial condition for the Milne function $\alpha(R)$ which defines $f=\alpha\sin\beta$ has been set to the usual WKB condition $\alpha(R_m)=1/\sqrt{K(R_m)}$ at $R_m=R_e$, where $K'(R_e)=0$. Well away from threshold we can expect the Milne function to follow this behavior to infinity $\alpha(R)\approx 1/\sqrt{K(R)}\rightarrow 1/\sqrt{k}$, and $C^{-1}\rightarrow 1$. However, as we approach threshold $C^{-1}(\varepsilon)$ begins to decrease and ultimately exhibits the limiting behavior in Table II. Viewed from an asymptotic perspective, the normalizable function $s(\varepsilon,R)$ begins to experience a partial reflection due to the long-range potential, and has difficulty in penetrating to short distances. As a consequence the amplitiude of the function in the vicinity of R_m is diminished to $s(\varepsilon,R_m)\rightarrow[C^{-1}/\sqrt{K(R_m)}]\sin\beta(R_m)$. Presumably the amplitude of the channel is already diminished in the vicinity where the close coupling has generated the quantity $[\overline{\mathbf{Y}}_{OO}^{-1}-\tan\lambda_O]^{-1}$ in Eq. (1.6) and the matrix $\overline{\mathbf{R}}_{OO}$ is reduced accordingly.

From Eq. (4.1b) we find that the energy dependence of the *elastic* scattering elements $T_{i,i}$ depends both on C_i^{-2} and on the scattering phase shift ξ_i for the closing channel,

$$T_{i,i}=(1-e^{i2\xi_i})-2iC_i^{-2}e^{i2\xi_i}[\overline{\mathbf{Y}}_{OO}^{-1}-(\tan\lambda_O+iC_O^{-2})]_{i,i}^{-1}, \quad (4.2)$$

Both these parameters in turn are defined by the well-behaved analytic reference function $f(\varepsilon,R)\rightarrow C(E)s(\varepsilon,R)$ associated with channel $|i\rangle$, since the asymptotic form of $s(\varepsilon,R)$ yields the phase shift. As seen in Table II, for low partial waves the threshold behavior for the scattering phase shift $\xi(\varepsilon)$ exactly mimics C^{-2}, i.e., $\xi\rightarrow(-A_l k)^{2l+1}$. However, depending on the leading power R^{-s} of the long-range potential in Eq. (2.3), the higher partial waves will begin to deviate from the C^{-2} behavior, i.e., $\xi\rightarrow(A_s k)^{s-2}$, whenever $(2l+1)>(s-2)$.

Examples of these various dependences for the diagonal matrix elements $|T_{ii}|^2$ are given in Fig. 5 for $l=0$, 2, and 4 channels. Channels 1, 2, and 3 are strongly open, and these elements remain essentially constant in the vicinity of the 2+2 threshold. The $|T_{44}|^2$ element rises like k^2, as expected for an incident $l=0$ channel. Both the $|T_{55}|^2$ element with $l=2$ and the $|T_{66}|^2$ element with $l=4$ are very small, and show the appropriate k^2 at threshold due to long-range C_{ii}/R^3 contributions in their reference potentials. As we see in Eq. (1.7), the next leading term in the asymptotic reference potentials varies as $1/R^6$. Note that at about $E=100\,\mu$K the $|T_{55}|^2$ element switches to a k^8 dependence, indicating that the $s=6$ dependence adds to the phase shift and now dominates over the $s=3$ contribution. The $|T_{66}|^2$ element exhibits the same phenomena at $E=1000\,\mu$K, but in this case there is a distructive interference between the two contributions and the element dips toward zero in this region. This behavior is consistent with the relative signs of the C_3 and C_6 coefficients in Eq. (2.7) for these two channels.

For single-channel s-wave scattering, where $\xi(\varepsilon)\rightarrow -A_0 k$ in Table II, the parameter A_0 is the scattering length defined by the chosen reference potential. The sign and magnitude of A_0 is a sensitive function of the position of the last bound state supported by the reference potential. This is, of course, given by the condition $\nu(\varepsilon_n)=n\pi$. In fact, an analytic relationship exists between the s-wave scattering length A_0 and Milne bound-state phase $\nu(0)$ evaluated at threshold [4],

$$A_0=-\left.\frac{\partial\nu}{\partial\kappa}\right|_{\kappa\rightarrow 0}\left[\cot\left(\frac{\pi}{s-2}\right)+\cot\nu(0)\right], \quad (4.3)$$

where $\varepsilon=-\hbar^2\kappa^2/2\mu$. The parameter s in $\cot(\pi/(s-2))$ is defined by the leading asymptotic power law C_s/R^s for the potential. This expression has been used [4] to derive some general relations between the position of bound states predicted by $\nu(\varepsilon_n)=n\pi$ and the scattering length. If a bound state $\varepsilon_n=-\hbar^2\kappa_n^2/2\mu$ lies just *below* threshold, then $\nu(0)\approx n\pi-(\partial\nu/\partial\kappa)\kappa_n$ and $A_0\rightarrow 1/\kappa_n$. However if $\nu(0)\approx n\pi+(\partial\nu/\partial\kappa)\overline{\kappa}_n$, then we can imagine a pseudo-bound-state existing at a positive energy $\overline{\varepsilon}_n=+\hbar^2\overline{\kappa}_n^2/2\mu$ just *above* threshold, and $A_0\rightarrow -1/\overline{\kappa}_n$.

Since the quantity $-\partial\nu/\partial\kappa|_{\kappa\rightarrow 0}$ is basically an asymptotic property that only depends on the asymptotic form of the reference potential C_s/R^s, and is independent of

any variations in the shorter-range terms in Eq. (2.7), it can be shown to scale as $\beta_s=(2\mu|C_s|/\hbar^2)^{1/(s-2)}$. All ground-state alkali-metal-atom interactions are dominated by the C_6/R^6 in Eq. (2.7) with both the $a\ ^3\Sigma_u$ and the $X\ ^1\Sigma+_g$ potentials having the same C_6, and we have $\cot[\pi/(s-2)]=1$. The authors of Ref. [12] found that for such potentials $-\partial\nu/\partial\kappa\to 0.477\beta_6$, which agrees perfectly with our calculations for both ^{23}Na and ^{87}Rb collisions. An expression completely analogous to Eq. (4.3) was first derived by Gribakin and Flambaum [23] using a semiclassical expression to define the phase $\nu(0)$. This semiclassical approach was further refined in Ref. [24] to obtain the effective range behavior, and applied to cold atom scattering. Based on Eq. (20) in Ref. [24], we can replace their semiclassical phase $\Phi-\pi/2(s-2)$ with $\nu(0)+\pi/2$, and retrieve Eq. (4.3), with $-\partial\nu/\partial\kappa$ being defined analytically as follows:

$$-\frac{\partial\nu}{\partial\kappa}=\sin\left(\frac{\pi}{s-2}\right)(s-2)^{-2/(s-2)}\frac{\Gamma\left(\frac{s-3}{s-2}\right)}{\Gamma\left(\frac{s-1}{s-2}\right)}\beta_s. \quad (4.4)$$

For $s=6$, this predicts $-\partial\nu/\partial\kappa\to 0.478\beta_6$, and confirms our numerical results. The same behavior is predicted in Eq. (9) of Ref. [22], with $K^0_{l=0}(0)\equiv\tan[\nu(0)+\pi/2]$. The s-wave coefficent $C^{-2}\to -B_0k$ obeys a similar threshold dependence as $\xi(\varepsilon)\to -A_0k$, and we can use the expressions in Table II to derive an analogous relationship for B_0,

$$\frac{C^{-2}}{k}\to B_0=-\left.\frac{\partial\nu}{\partial\kappa}\right|_{\kappa\to 0}\sin^{-2}\nu(0)\equiv-\left.\frac{\partial\nu}{\partial\kappa}\right|_{\kappa\to 0}\cos^{-2}\lambda(0), \quad (4.5)$$

which again is well confirmed by our numerical calculations.

B. Cusp behavior at channel closings

A simple example of threshold and cusp effects for $l=0$ channels is demonstrated by the $|T_{11}|^2$, $|T_{14}|^2$, and $|T_{44}|^2$ elements associated with $F=0$, $p=+1$ case in Table I(a). These two channels with $(l,f)=(0,0)$ are strongly coupled at short range by exchange interactions, and, as expected for an $l=0$ channel, the element $|T_{14}|^2\propto k_4$ and $|T_{44}|^2\propto k_4^2$ as channel 4 closes at $E/E_{HF}=2$. This was already demonstrated in Figs. 4 and 5. Furthermore we see in Fig. 1 that as channel 4 closes a cusp appears in the $|T_{11}|^2$ matrix element. This is shown in more detail in Fig. 6, and again we find that this behavior is reproduced perfectly by the GMQDT analysis. An analysis of a two-channel cusp was given in Appendix A of Ref. [9]. We only expect a pronounced cusp behavior when the closing channel, such as channel 4 in this case, corresponds to an s-wave channel with $l=0$. It is simply related to the energy variation of the four GMQDT parameters ξ, $\tan\lambda$, C^{-2}, and ν, as given in Table II. The approach of $|T_{11}|^2$ to threshold from below as $\varepsilon\to 0^-$ depends on $\partial\nu_4/\partial\varepsilon$, which we can obtain from Eq. (4.4), while from above $\varepsilon\to 0^+$ it depends on both $\partial\lambda_4/\partial\varepsilon$ and $\partial C_4^{-2}/\partial\varepsilon$.

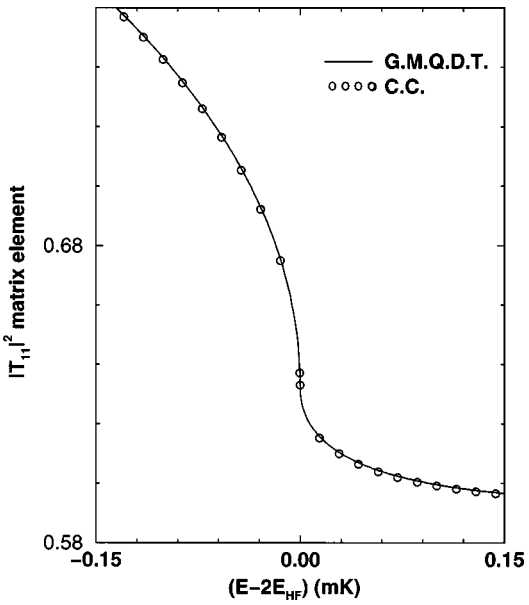

FIG. 6. Six-channel ($F=0$, $p=+1$) case. There is a cusp behavior in $|T_{11}|^2$ for channel 1 ($l=0$) at the opening of channel 4 ($l=0$). Very close to threshold the open channels 5 ($l=2$) and 6 ($l=2$) are effectively treated as closed. This is because the classically accessible regions beyond the centrifugal barrier occur well beyond $R_{\max}=70\,000$ a.u.

These limiting forms, combined with the threshold constraint $\tan\lambda(0)\tan\nu(0)=-1$, allow us to easily evaluate the cusp behavior.

C. Perturbative corrections for weak long-range spin-spin couplings

The terms proportional to α^2R^{-3} in Eqs. (2.7b) and (2.7c) are the so-called spin-spin (SS) interactions [3,19], which are second order in the fine-structure constant α. Because the SS terms persist to such large distances, we can expect a slower convergence of the **Y** matrix elements associated with such couplings. As we shall see shortly, higher-order long-range SS interactions dominate the coupling when channel 6 is open. Such long-range behavior is especially evident in the $Y_{5,6}$ element in Fig. 7, which, even well above threshold, is not yet converged at 200 a.u. Examining Table 1(a) we see that $Y_{5,6}$ involves coupling between a pair of asymptotically *degenerate* channels with orbital angular momenta l differing by 2. In the Born approximation we can expect these weakly coupled elements to be proportional to $Y_{i,j}\propto\langle j_l(kR)|\alpha^2R^{-3}|j_{l+2}(kR)\rangle$, which is a very slowly converging integral and leads to this boring behavior. Furthermore, as the energy is lowered the Bessel functions in the integrand penetrate more deeply into nonclassical regions, and we must be on guard for significant energy variation in these particular long-range **Y** matrix elements.

In Eq. (1.7) we designate the scattering matrix elements generated by the short-range **Y** matrix in Eq. (1.5) as $\mathbf{S}_{OO}(\mathbf{Y})$, and use the distorted-wave approximation (DWA) in Eq. (1.8) to apply a perturbative long-range correction $S^{\rm DWA}_{i,j}=-2\pi i\langle\varepsilon_i|C_{i,j}/R^3|\varepsilon_j\rangle$ to these elements, where the

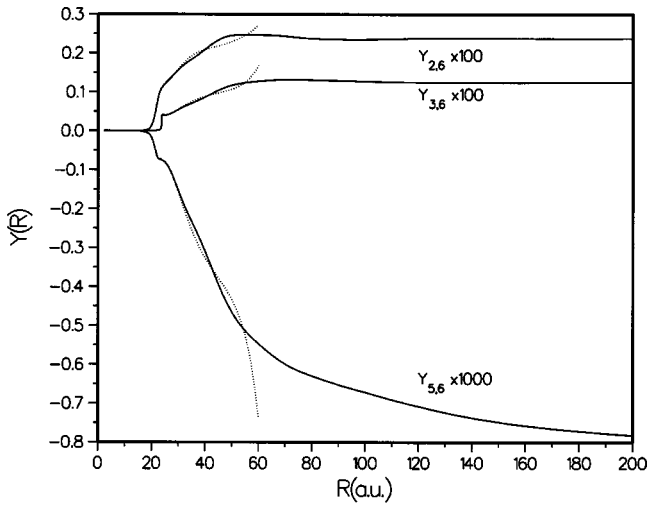

FIG. 7. R dependence of spin-spin-coupled $Y_{26}(R)$, $Y_{36}(R)$, and $Y_{56}(R)$ elements for the six-channel ($F=0$, $p=+1$) case. Solid curves are for a kinetic energy $\varepsilon=0.0818\,\mathrm{cm}^{-1}$ above the $f_a=2$, $f_b=2$ threshold. Dashed curves are for $\varepsilon=0.00181\,\mathrm{cm}^{-1}$.

energy-normalized continuum states are given by the asymptotically defined reference functions, $|\varepsilon_i\rangle = (2\mu/\pi\hbar^2)^{1/2} s_i(\varepsilon_i,R)$ in Eq. (3.7a), obtained in the mixed representation using adiabatic reference potentials defined by each subset of (f,l) channels. This integral can be evaluated numerically, and has been found to yield excellent results. However, for degenerate channels, when *both* reference functions approach the Bessel function $s_i(\varepsilon_i,R)\rightarrow J_i(\varepsilon_i,R) \rightarrow k_i^{-1/2}\sin(k_iR-\pi l/2)$, we retrieve the simple Born approximation which can be evaluated analytically. For an $l\rightarrow l+2$ transition we obtain

$$S_{i,j}^{\mathrm{DWA}}(l=0)\rightarrow -i7.63209\sqrt{\varepsilon_i(\mu K)}C_{i,j}\ \text{a.u.}, \quad (4.6a)$$

$$S_{i,j}^{\mathrm{DWA}}(l=1)\rightarrow -i0.848267\sqrt{\varepsilon_i(\mu K)}C_{i,j}\ \text{a.u.}, \quad (4.6b)$$

$$S_{i,j}^{\mathrm{DWA}}(l=2)\rightarrow -i0.424084\sqrt{\varepsilon_i(\mu K)}C_{i,j}\ \text{a.u.}, \quad (4.6c)$$

This implies a *universal* k^2 threshold dependence for all $|T_{ij}|^2$ elements involving degenerate channels that are dominated by long-range spin-spin couplings.

Confirmation of this behavior can be seen in Fig. 8, where we plot the only three matrix elements $|T_{11}|^2$, $|T_{22}|^2$, and $|T_{12}|^2$ that are open at the ($f_a=1$, $f_b=1$) threshold. The diagonal elements are given perfectly by the pure MQDT scattering matrix $\mathbf{S}_{OO}(\mathbf{Y})$ in Eq. (1.7). The $|T_{11}|^2$ element has the k^2 dependence we expect for an s-wave channel, while $|T_{22}|^2$ begins as k^2 because of the long-range R^{-3} dependence of the reference potential for this d-wave channel, but then switches over to the k^8 dependence associated with a R^{-6} potential combined with an $l=2$ partial wave. However, the $|T_{12}(\mathbf{Y})|^2$ element in Fig. 8 exhibits the typical k^6 dependence predicted by Eq. (1.6) for an s- to d-wave transition if the interaction matrix element V_{12} were short ranged, and is much too small compared to the close-coupled results which give the k^2 dependence predicted by Eq. (4.6a).

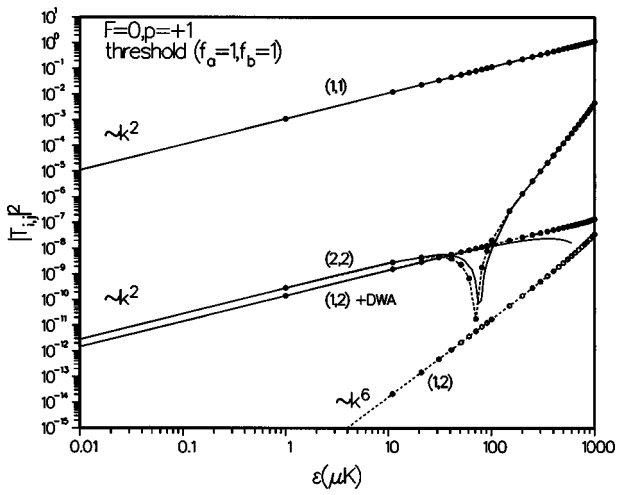

FIG. 8. $|T_{ij}|^2$ elements for the six-channel ($F=0$, $p=+1$) case. ε is measured relative to the $f_a=1$, $f_b=1$ threshold, where only $\alpha=1$ and 2 channels are open. Solid curves indicate CC results. Dashed curves with solid dots show the excellent agreement when the perturbative SS correction $\mathbf{S}(\mathbf{Y})+\mathbf{S}^{\mathrm{DWA}}$ in Eq. (1.7) is applied to $|T_{12}|^2$. The dashed curve with open circles shows the $|T_{12}(\mathbf{Y})|^2$ element by itself, which appropriately varies as k^6 but is negligible compared to $|T_{12}^{\mathrm{DWA}}|^2$.

By evaluating Eq. (4.6a) and adding this to $S_{12}(\mathbf{Y})$ in Eq. (1.7), we obtain perfect agreement with the close-coupled results, as seen in Fig. 8.

For some of the very small spin-spin matrix elements we find an interesting second-order approximation which is very precise. This is shown in Fig. 9 for the elements $|T_{45}|^2$, $|T_{56}|^2$, and $|T_{46}|^2$ that open at the ($f_a=2$, $f_b=2$) threshold. The close-coupled results for both $|T_{45}|^2$ and $|T_{56}|^2$ are in

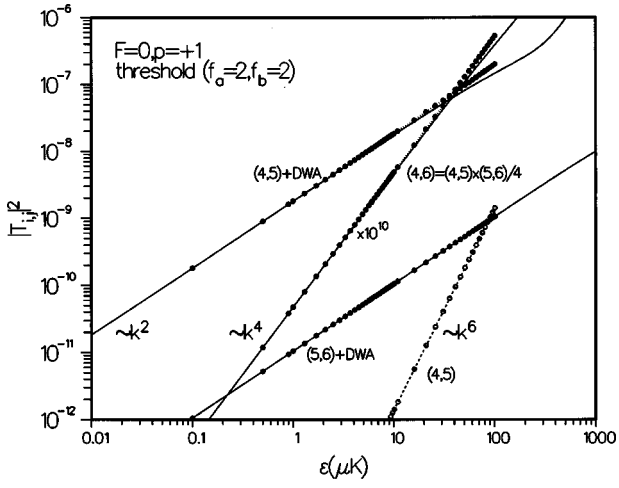

FIG. 9. $|T_{ij}|^2$ elements for the six-channel ($F=0$, $p=+1$) case. ε is measured relative to the $f_a=2$, $f_b=2$ threshold where all channels are open. The solid curves indicate CC results. The dashed curve with solid dot shows results using $\mathbf{S}(\mathbf{Y})+\mathbf{S}^{\mathrm{DWA}}$ in Eq. (1.7), and the second-order correction in Eq. (4.7) is used to evaluate $|T_{45}|^2$, $|T_{56}|^2$, and $|T_{46}|^2$. The dashed curve with open circles shows the $|T_{45}(\mathbf{Y})|^2$ element by itself, which appropriately varies as k^6 but is negligible compared to $|T_{45}^{\mathrm{DWA}}|^2$.

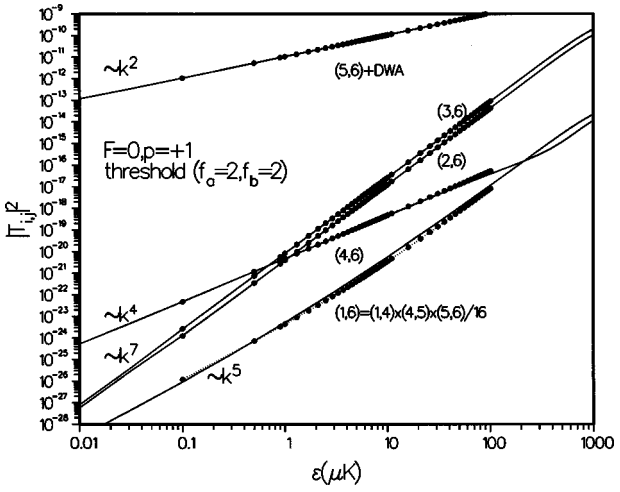

FIG. 10. $|T_{ij}|^2$ elements for the six-channel ($F=0$, $p=+1$) case. ε is measured relative to the $f_a=2$, $f_b=2$ threshold where all channels are open. The solid curves indicate CC results. The dashed curves with solid dot shows result using the $\mathbf{S}(\mathbf{Y})+\mathbf{S}^{\mathrm{DWA}}$ correction in Eq. (1.7) and the second-order correction in Eq. (4.8). The element $|T_{16}|^2$ has a k^5 dependence consistent with a third-order process, and is well represented by the approximation $|T_{16}(\mathrm{sequence})|^2=|T_{14}|^2|T_{45}|^2|T_{56}|^2/16$.

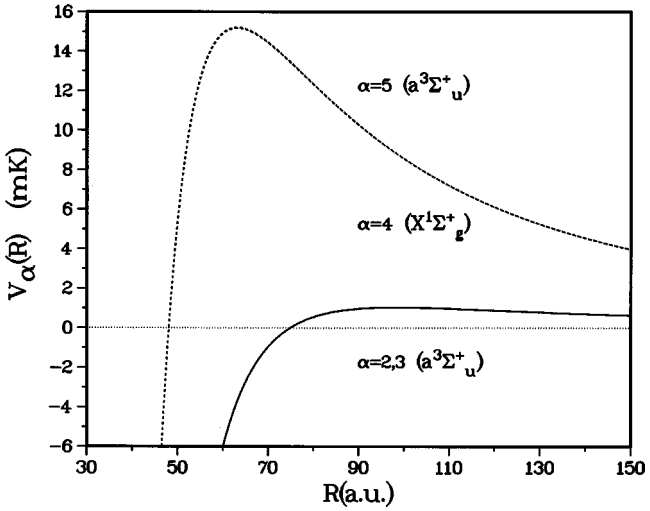

FIG. 11. Asymptotic correlation of the ($F=1$, $p=-1$) channels $\alpha=2$, 3, 4, and 5 which dissociate to the $f_a=1$, $f_b=2$ threshold at $E=0$. Channel 4 adiabatically correlates with the $X\ ^1\Sigma_g^+$ potential at short distances, while the remaining three channels all adiabatically correlate with $a\ ^3\Sigma_u^+$ at small R.

excellent agreement with the first-order predictions of Eqs. (4.6a) and (4.6c), respectively. However, since the angular moment l for channels 4 and 6 differ by 4, there is no direct spin-spin coupling between these states. However, they can be coupled by the sequence $4\rightarrow5\rightarrow6$, and we predict

$$|T_{i,k}^{\mathrm{DWA}}(l\rightarrow l+4)|^2=|T_{i,j}^{\mathrm{DWA}}(l\rightarrow+2)|^2\times|T_{j,k}^{\mathrm{DWA}}(l+2\rightarrow l+4)|^2/4. \quad (4.7)$$

This expression can be derived from the half-collision amplitude theory [28] we developed based essentially on GM-QDT. The exquisite agreement between this expression and the exact close coupling is demonstrated in Fig. 9. Since $|T_{45}|^2$ and $|T_{56}|^2$ each vary as k^2, we find that the overall threshold dependence of the $|T_{46}|^2$ element is k^4, as implied by the product in Eq. (4.7). This expression is *not* dependent on perturbation theory, but rather relies on the fact that the sequence of transitions occur in different regions of internuclear separation. It is a special application of the more general result.

$$|T_{i,k}(\mathrm{sequence})|^2=|T_{i,j}(\mathrm{inner})|^2|T_{j,k}(\mathrm{outer})|^2/4. \quad (4.8)$$

If there are competing pathways there are complicated interferences that must be introduced, but for present applications Eq. (4.7) is quite adequate.

A final demonstration of Eq. (4.7) is observed in the element $|T_{16}|^2$ in Fig. 10, where the sequence of half-collision amplitude transitions is actually carried to third order. First we note that $|T_{45}|^2$ and $|T_{56}|^2$ vary as k^2, in quantitative agreement with the DBA predictions in Eq. (4.6). Furthermore $|T_{46}|^2$ varies as k^4, and equals the second-order expression $|T_{45}|^2|T_{56}|^2/4$ given by Eq. (4.7). Finally we find that $|T_{16}|^2=|T_{14}|^2|T_{46}|^2/4$ varies as k^5, and follows the sequence $1\rightarrow4\rightarrow6$ predicted by Eq. (4.8). In this case the $|T_{14}|^2$ element is due to exchange coupling and is given by the short-range $|T_{14}(\mathbf{Y}\})|^2$, which varies as k. Since $|T_{46}|^2$ is already shown to follow the sequence $4\rightarrow5\rightarrow6$ we see that $|T_{16}|^2=|T_{14}|^2|T_{45}|^2|T_{56}|^2/16$, and the inelastic transition from channel 1 to channel 6 follows the third-order pathway $1\rightarrow4\rightarrow5\rightarrow6$.

D. Frame transformation analysis of *l*-degenerate channel couplings

So far all the long-range SS couplings we have considered in the $F=0$, $p=+1$ block of channel states in Table I(a) have involved channels which differ in both their channel spin state quantum number f and in their nuclear angular momentum state l. However, in collisions involving hyperfine transitions, we often encounter SS coupling between asymptotically degenerate channel states which differ by the channel state quantum number f, but which have identical l. Examining the block of channel states in Table I(b) for $F=1$ and $p=-1$ we see this situation occurs between channels 2 and 3 with $l=1$ and between channels 4 and 5 with $l=3$. All four channels asymptotically correlate with the ($f_a=1$, $f_b=2$) threshold, and the long-range portion of the reference potentials we will use for these channels are shown in Fig. 11. These reference potentials $\mathbf{V}^O$ correspond to the mixed basis we discussed in Sec. III, where the four $l=1$ channels and the three $l=3$ channels in Table I(b) are diagonalized separately, using an orthogonal matrix $\mathbf{M}(R)=\begin{bmatrix}\mathbf{M}_{l=1}(R) & 0\\ 0 & \mathbf{M}_{l=3}(R)\end{bmatrix}$, which preserves the indentity of the angular momentum quantum number l. The comparable matrix for the $F=0$, $p=+1$ channels approaches the unit matrix as $R\rightarrow\infty$, and the associated reference potentials preserve the asymptotic identity of the channel spin states f. However, because SS coupling between the l-degenerate

channel states in the $F=1$, $p=-1$ block persists out to infinity, the orthogonal matrix $\mathbf{M}(\infty)\neq 1$ is no longer a unit matrix and the reference potentials correlate with *rotated* sets of the channel states. We will show how the asymptotic matrix $\mathbf{M}(\infty)$ defines a simple frame transformation that we can use, in combination with our MQDT theory, to obtain an accurate reproduction of the close-coupled results.

The scattering matrix $S_{\gamma,\gamma'}$ we require to describe the cross sections and rate for the hyperfine transitions for Na+Na must be constructed in an asymptotic basis using the well-defined channel quantum states $j=l,f,f_a,f_b$ in Eq. (2.1) and Table I. We often refer to these as the case e basis, because of their analogy to the Hund's case (e) angular momentum coupling scheme used in diatomic spectroscopy [29], and we will specify the particular interaction matrix in Eqs. (2.2) and (2.3) as $\mathbf{W}$(case e), and we specify the resultant scattering matrix in Eq. (2.6) as $\mathbf{S}$(case e).

In performing the CC calculations for $F=1$ and $p=-1$ we have two equally valid options. First we can integrate Eq. (2.1) explicitly using $\mathbf{W}$(case e) to obtain $\mathbf{K}$(case e) in Eq. (2.5), and thus directly evaluate $\mathbf{S}$(case e) using Eq. (2.6). Of course in this basis the *l*-degenerate channels have *off-diagonal* R^{-3} couplings which persist in contributing to the scattering out to extremely large distances. To achieve convergence on spin-spin elements we find we must often integrate out to $R>10\,000$ a.u. or more [see Ref. [30] for a discussion of similar long-range concerns for the R^{-3} polarization potential in H^++F collisions]. This is no problem if one uses amplitude following algorithms, such as the Gordon method [31], but it does restrict the numerical options at one's disposal.

An alternative close-coupled approach (which we find is *critical* to use in our MQDT analysis) is to perform the calculations in a rotated basis of channel states, which removes the *asymptotic* R^{-3} couplings, and use the following rotated interaction matrix in the close-coupled equations (2.1):

$$\mathbf{W}(\mathrm{rot},R)=\mathbf{M}(\infty)\,W(\mathrm{case\ e},R)\,\tilde{\mathbf{M}}(\infty), \tag{4.9}$$

Note that the off-diagonal elements $W_{2,3}$(rot) and $W_{4,5}$(rot) now vanish as R^{-6}, while the diagonal elements still vanish as R^{-3} and we achieve convergence of the $\mathbf{S}$(rot) matrix elements at much shorter distances. Thus if we use the mixed reference potentials to obtain the corresponding $\mathbf{Y}(\mathrm{rot},E,R)$ in Eq. (3.1), we can expect it will convergence at a conveniently small distance *R*, and we can use Eq. (1.5) to obtained a good representation of the close-coupled scattering matrix $\mathbf{S}$(rot). Numerically we find that the Y_{23}(rot) and Y_{45}(rot) elements, and their associated diagonal elements, are fully converged by $R=40$ a.u. Given $\mathbf{S}$(rot) we can then retrieve $\mathbf{S}$(case e) by a simple frame transformation at the conclusion of the calculation,

$$\mathbf{S}(\mathrm{case\ e})=\tilde{\mathbf{M}}(\infty)\mathbf{S}(\mathrm{rot})\mathbf{M}(\infty). \tag{4.10}$$

The excellent agreement between the close-coupled and MQDT results is illustrated in Fig. 12.

Note that Eq. (4.10) is a generalized version of the frame transformation theory [32] that has been applied so successfully to treat spin-exchange collisions involved $A(^2s)+B(^2s)$ atoms. For example, the frame transformation matrix $\mathbf{M}(\infty)$ consists of two 2×2 orthogonal matrices $\begin{bmatrix}\cos\varphi l & \sin\varphi l\\ -\sin\varphi l & \cos\varphi l\end{bmatrix}$ that are described by two separate *l*-dependent rotation angles φl. If we look at, say, the 2×2 block $\begin{bmatrix}S_{4,4} & S_{4,5}\\ S_{5,4} & S_{5,5}\end{bmatrix}$ of $\mathbf{S}$(rot), that will undergo the $\varphi l=3$ rotation, we see it is dominated by the diagonal elements $S_{i,i}\approx e^{i2\xi_i}$, and the resultant off-diagonal case e element essentially equals

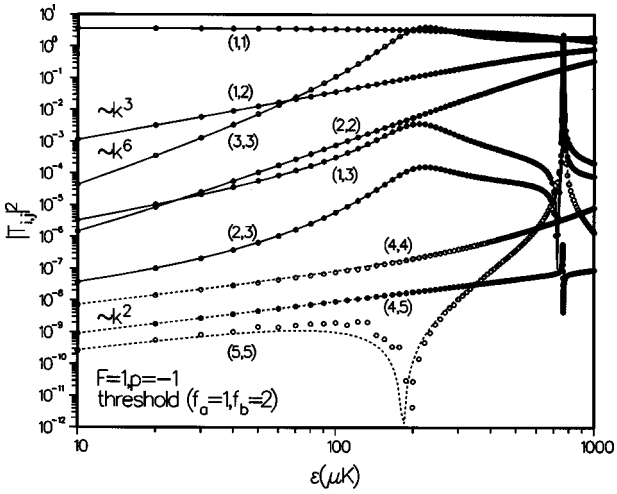

FIG. 12. $|T_{ij}|^2$ elements for the seven-channel ($F=1$, $p=-1$) case in Table I(b). ε is measured relative to the $f_a=1$, $f_b=2$ threshold, where five channels are open. As seen in Fig. 11, channels 2 and 3 with $l=1$ are degenerate, and channels 4 and 5 with $l=3$ are degenerate. The circles and dots indicate the exact CC results. The curves indicate the excellent results obtained by applying the frame transformation $\mathbf{S}(\mathrm{case\ e})=\tilde{\mathbf{M}}(\infty)\mathbf{S}(\mathrm{rot})\mathbf{M}(\infty)$ to the rotatated scattering matrix $\mathbf{S}$(rot) obtained with the GMQDT method. The elements shown in this figure are only those that are strongly coupled by the exchange interaction.

$$T_{4,5}(\mathrm{case\ e})=\cos\varphi_3\sin\varphi_3[e^{i2\xi_4(\mathrm{rot})}-e^{i2\xi_5(\mathrm{rot})}]. \tag{4.11}$$

Recall from Fig. 11 that $\alpha=4$ correlates with the $X\,^1\Sigma_g^+$ state at short distances, while $\alpha=5$ correlates with the $a\,^3\Sigma_u^+$ state, and we see that Eq. (4.11) depends on the *difference* between the elastic-scattering scattering phase shifts for the triplet and singlet molecular potentials. Thus Eq. (4.11) is identical to the well-known spin-exchange expression, which also involves such a difference [32]. The result for this one special element is consistent with our previous study of the loss rates in cold ^{87}Rb+^{87}Rb collisions [4], where we found extremely small loss rates because the scattering lengths, and hence the phase shifts for the Rb_2 triplet and singlet potentials were almost identical. Equation (4.11) is good confirmation of that effect.

V. DISCUSSION AND CONCLUSIONS

We have presented an analysis of threshold effects based on GMQDT, which gives an exact analytic representation of

the multichannel threshold laws, and yields results which are numerically equivalent to the close-coupled results for those channels that are strongly coupled at short range. The very long-range spin-spin interactions are analyzed using the distorted-wave approximation in Eq. (1.7), and the result gives us a complete quantitative description of all threshold laws associated with the hyperfine transitions in ultracold atomic collisions.

In general the scattering matrix $\mathbf{S}_{OO}(E)$ and the associated transition matrix $\mathbf{T}_{OO}(E)=1-\mathbf{S}_{OO}(E)$ vary rapidly with energy. Thus direct numerical integration of the close-coupled equations (2.2), while always giving exact results, must be performed over a narrow grid of energies and expensive searches must be performed, especially if unanalyzed resonance structure is present. (This is demonstrated by the CC data points in Fig. 1.) Furthermore, brute force integration does not offer any insight into the threshold behavior of the resultant cross sections and rates. However, if the coupling in our system occurs predominantly in classically accessible regions where the diagonal elements of $E-\mathbf{W}(R)>0$ are positive, it is preferable to use the GMQDT expansion of the CC wave function in Eq. (3.1). With a careful choice of a diagonal set of reference potentials $V(R)$ which reflect the long-range properties of the interaction matrix in Eq. (2.3), we expect that, except near threshold, the dominant energy variations in $\mathbf{S}_{OO}$ can be associated with the diagonal set of phase shifts $\xi_O(E)$ for open channels, and the bound-state phase shifts $\nu_C(E)$ for closed channels defined by $V(R)$.

As we approach threshold from above two additional parameters $C_O(E)$ and $\lambda_O(E)$ come into play, and dominate the threshold behavior. The associated matrix $\mathbf{Y}(E)$ varies almost monotonically with energy, and we can substantially and sometimes profoundly reduce the number of close-coupled calculations we must perform to describe a given process. Essentially we use reference potentials which effectively go well beyond the leading asymptotic term provided by $l(l+1)/R^2$, and can do a good job of describing the ''elastic'' scattering in each channel. If $\mathbf{Y}$ is almost constant the systematics of the energy structure is simply related to the single-channel parameters that occur in analytic expression (1.5) for $\mathbf{S}_{OO}$.

In addition to the obvious, but rather mundane, economic advantage of the GMQDT analysis in performing close-coupling calculations even when all channels are open, the theory becomes truly interesting as we approach thresholds where various channels begin to close. In this region two very important and closely related energy-dependent effects become significant. First, whenever $\varepsilon_i<0$ and a channel becomes completely closed, both reference functions f_i and g_i become asymptotically divergent, and the well-behaved linear combination given in Eq. (3.4) manifests inself as a closed-channel resonance. Resonances are approximately located at the poles of the matrix $[\tan\nu_C(E)+\mathbf{Y}_{CC}]^{-1}$ where the zeros of the bound-state phase $\tan\nu_C(E)=0$ locate the bound-state eigenvalues in the closed channels, and $\mathbf{Y}_{CC}$ introduces shifts in the resonance positions induced by the close coupling. Note that $C(E)$ is extremely sensitive to tunneling through the rotational barriers, and gives a powerful means of isolating the effects of shape resonances in a multichannel problem. Close to threshold an interesting ''multichannel'' shape resonance effect is introduced by the energy variation of $\tan\lambda_O$ that appears in the denominator of Eq. (6). In addition, the behavior of $C^{-1}(E)$ for $l=0$ at threshold is directly related to what have been called ''zero-energy'' resonances [13]. These shape resonance phenomena will be presented in a subsequent resonance paper.

The second effect, which is the primary concern of this paper, is associated with the threshold behaviors just above and just below a channel closing. This is related to the energy dependence of the four MQDT parameters ξ, ν, λ, and C, which are defined for each channel. Their threshold dependences are summarized in Table II. Except at energies just *above* a threshold, the two phases $\xi(\varepsilon)$ and $\nu(\varepsilon)$ are in fact sufficient to perform a rather complete and rigorous GMQDT analysis of close-coupled wave functions, including, for example, many manifestations of overlapping and non-Lorentzian resonant structure. Below threshold we can always rely on Eq. (1.3) to be valid, even as $\varepsilon\rightarrow 0^-$ from below. However, as $\varepsilon\rightarrow 0^+$ from above the analytic reference functions, f and g begin to loss the asymptotic phase relationship implied by Eqs. (3.7), and their asymptotic behavior requires the introduction of the two additional QDT parameters $C(\varepsilon)$ and $\tan\lambda(\varepsilon)$ in Eq. (3.6) These appear in the analytic expression (1.4) which describes the scattering. For short-range interactions, this analysis leads to the threshold laws summarized in Table II which are well substantiated by the many comparisons made in Sec. IV.

Once again, it must be emphasized that the complete physics of the scattering problem is already dictated by the $N\times N$ interaction matrix $\mathbf{W}(R)$ that is used in solving the close-coupled equations. $\mathbf{Y}$ by itself has no intrinsic meaning, but rather is dictated by our *choice* of reference potentials $V_i(R)$. What GMQDT offers is an alternative set of *exact* solutions to the *same* set of close-coupled scattering equations which are constructed to be an analytic function of the total energy E. It converts the raw numerical output of the close-coupled scattering equations into a form which gives physical insight into the multichannel dynamics, especially in the presence of closed-channel resonances, or when multichannel Wigner threshold laws are of concern.

For those spin depolarization cross sections which are dominated by very weak long-range α^2R^{-3} couplings we must apply the Born approximation correction in Eq. (4.6), and we find a universal k^2 threshold dependence for all $|T_{ij}|^2$ elements associated with such transitions. In addition we have found that many transition matrix elements are quantatively represented as a *sequence* of first-order transitions, as expressed in Eqs. (4.7) and (4.8), and this is seen to persist even to third order. Finally, for spin-spin-coupled degenerate channels which have *identical* nuclear angular momenta l, we have introduced a simple frame transformation in Eq. (4.10) which removes the asymptotic coupling, and allows us to use short-range GMQDT expressions to obtain accurate results.

APPENDIX A: MILNE ANALYSIS OF GMQDT REFERENCE FUNCTIONS AND PARAMETERS

The relationships between the various reference functions are summarized in Table III. The analytic set (f,g) is adapted

TABLE III. Milne-based definition of various specialized reference functions. $W(a,b)=ab'-a'b$.

Analytic reference functions: analytic in ε across threshold, $W(g,f)=1$		
$f(\varepsilon,R)=\alpha\sin\beta \quad =Cs(\varepsilon,R)$	$\to 0$	$R\to 0$
$g(\varepsilon,R)=\alpha\cos\beta \quad =[C^{-1}c(\varepsilon,R)-(\tan\lambda)C(\varepsilon)s(\varepsilon,R)]$	$\to\infty$	$R\to 0$
Continuum functions: $\varepsilon>0$, $W(c,s)=1$		
$s(\varepsilon,R)=C^{-1}f(\varepsilon,R) \quad =\frac{\alpha}{C}\sin\beta$	$\to(\cos\xi)J+(\sin\xi)N$	$R\to\infty$
$c(\varepsilon,R)=C[g(\varepsilon,R)+(\tan\lambda)f(\varepsilon,R)] \quad =\frac{\alpha}{C\cos\lambda}\cos(\beta+\lambda)$	$\to(\sin\xi)J+(\cos\xi)N$	$R\to\infty$
Asymptotically well-behaved closed-channel function[a]: $\varepsilon<0$		
$\phi(\varepsilon,R)=[f(\varepsilon,R)\cos\nu-g(\varepsilon,R)\sin\nu] \quad =\alpha\sin(\beta-\nu)$	$\to\exp(-\lvert k\rvert R)$	$R\to\infty$
$\nu(\varepsilon)=\int_0^\infty dR/\alpha^2(\varepsilon,R)$	$\nu(\varepsilon)\to n\pi$ as	$\varepsilon\to\varepsilon_n$
WKB limit: if $\varepsilon\gg 0$, $C(\varepsilon)\to 1$, $\tan\lambda(\varepsilon)\to 0$		
f(ε,R)=Cs(ε,R)	→s(ε,R)	ε>
g(ε,R)=[C−1c(ε,R)(tan λ)Cs(ε,R)]	→c(ε,R)	ε>

[a] $\phi(\alpha,R)$ is generally divergent as $R\to 0$. True bound states occur whenever $\nu(\alpha)=n\pi$.

to the short-range portion of the reference potential, with boundary conditions set in the classically allowed regions. This insures that these functions are analytic in energy across threshold. The close-coupled wave function is analyzed with this set and the analytic $\mathbf{Y}(E)$ matrix is obtained.

In place of our previous analysis [8] of the reference functions in GMQDT, we shall use the more versatile Milne construction [10–12] to define the analytic reference functions,

$$f(R)=\alpha(R)\sin\beta(R), \tag{A1}$$

$$g(R)=\alpha(R)\cos\beta(R). \tag{A2}$$

Note that $f(\varepsilon,R)$ plays a central role in GMQDT, since it is uniquely defined to be that *particular* solution of the homogeneous second-order equation, $[d^2/dR^2+K^2(\varepsilon,R)]f(\varepsilon,R)=0$, which is *well behaved* as $R\to 0$. This equation is prescribed by the reference potential $V(R)$ we choose to associate with the given channel such that $K^2(\varepsilon,R)=2\mu[E-V(R)]/\hbar^2\to 2\mu\varepsilon/\hbar^2\to k^2$. The irregular function $g(\varepsilon,R)$ is also a solution to this equation, and together they form a particular pair of *independent* solutions at asymptotic kinetic energy ε with a Wronskian prescribed to be $f'g-g'f=1$. The independent solution g, is always divergent as $R\to 0$.

Although only two independent solutions can exist, these can be used to define an infinite variety of special solutions which satisfy useful boundary conditions, such as those defined in Table III. *All* such solutions are uniquely specified by the single amplitude $\alpha(\varepsilon,R)$ and the associated phase $\beta(\varepsilon,R)$ defined by the inhomogeneous Milne equation:

$$[d^2/dR^2+K^2(E,R)]\alpha(\varepsilon,R)=\alpha^{-3}(\varepsilon,R). \tag{A3}$$

By definition the phase $\beta(\varepsilon,R)$ is related to the amplitude $\alpha(\varepsilon,R)$ as follows, $d\beta/dR\equiv 1/\alpha^2$. The constant of integration is chosen such that

$$\beta(\varepsilon,R)=\int_0^R dR/\alpha^2(\varepsilon,R'), \tag{A4}$$

which then insures that $f(\varepsilon,R)=\alpha\sin\beta$ is well behaved as $R\to 0$. At this point the pair of boundary conditions we must prescribe for $\alpha(\varepsilon,r)$ are still completely at our disposal, and will be chosen below to insure proper analytic behavior with ε, especially as we cross thresholds.

In the vicinity just above a dissociation threshold we introduce a second set of reference functions (s,c) which is specifically adapted to describe the asymptotic scattering properties of *open* channels, using the usual asymptotic boundary conditions given in Eq. (3.7). In this appendix we explain the numerical procedures used to determine the connection between these two sets of reference functions. This connection is characterized by the three MQDT parameters ξ, C, and $\tan\lambda$ which appear in Eq. (3.8).

Except at specific eigenvalues, the analytic functions f and g for closed channels both contain an exponentially rising term as $R\to\infty$, i.e., $f=(\sin\nu)Ae^{+\kappa R}+(\cos\nu)Be^{-\kappa R}$, and $g=(\cos\nu)Ae^{+\kappa R}-(\sin\nu)Be^{-\kappa R}$. Our chore is to find the particular phase $\nu(\varepsilon)$ in Eq. (3.4) which insures that the well-behaved function $\phi(\varepsilon,R)=\alpha\sin(\beta-\nu)$ decays asymptotically. The bound states associated with the reference potential are defined by the condition $\sin\nu(\varepsilon_n)=0$, which insures that the reference function $f(\varepsilon_n,R)$ is well behaved at both $R=0$ and $R=\infty$. We will define the modular-π bound-state phase such that $\nu(\varepsilon_n)=n\pi$ is a measure of the number of nodes in the function $f(\varepsilon_n,R)$.

Given *any* initial values for $\alpha(\varepsilon,R_m)$ and its derivative $\alpha'(\varepsilon,R_m)$, we can always obtain an exact numerical solution to the Milne equation (A3), and the resultant reference functions are completely defined. Further, this formulation has the important feature that *any* particular solution to the Milne equation will give an energy-dependent bound-state phase integral

$$\nu(\varepsilon)=\int_0^\infty dR/\alpha^2(\varepsilon,R) \tag{A5}$$

which insures that the solution $\phi(\varepsilon,R)=\alpha\sin(\beta-\nu)$

$=\alpha\sin[\int_R^\infty dR'/\alpha^2(\varepsilon,R')]\to 0$ is well behaved at $R\to\infty$. For energies $\varepsilon<0$, the condition $\nu(\varepsilon_n)=n\pi$ is only satisfied at discrete eigenenergies $\varepsilon=\varepsilon_n$ where the solution $f(\varepsilon,R)$ is equivalent to the solution $\phi(\varepsilon,R)$. At such energies both f and ϕ are well behaved at both $R=0$ and $r=\infty$, and represent a single normalizable bound-state solution, or eigenfunction, of $[d^2/dR^2+K^2(\varepsilon_n,R)]\ f(\varepsilon_n,R)=0$. All the irregular character has been isolated in the single, unphysical solution g, which can then be rejected.

As discussed by Pan and Mies [33] we usually set our *initial* boundary conditions on $\alpha(\varepsilon,R_m)$ and $\alpha'(\varepsilon,R_m)$ at the equilbrium distance $R_m=R_e$ defined by the minimum in the reference potential where $dV(R)/dR|_{R_e}=0$, and choose them to have the following WKB-like initial values.

$$\alpha(\varepsilon,R_e)\approx 1/\sqrt{K(\varepsilon,R_e)}, \tag{A6a}$$

$$\alpha'(\varepsilon,R_e)\approx 0,. \tag{A6b}$$

Since $K(\varepsilon,R_e)$ is analytic in E throughout the range $V(R_e)<E<\infty$, the functions $\alpha(\varepsilon,R)$ and $\beta(\varepsilon,R)$ and the resultant reference functions $f(\varepsilon,R)$ and $g(\varepsilon,R)$ are analytic in E over this range as well, and especially across the important threshold region. To have Eq. (A1) perfectly consistent with WKB-like behavior in the vicinity of $R\approx R_e$, the Milne equation (A3) implies that $K^2\alpha\gg\alpha''$ at R_e. A more self-consistent scheme we have often used is to choose R_m to coincide with the condition $d^2[K^{-1/2}(E,R)]/dR^2|_{R_m}=0$, and then set the initial condition $\alpha'(\varepsilon,R_m)\approx d[K^{-1/2}(E,R)]/dR|_{R_m}$. This is a very useful choice for electronic reference functions which are often not very WKB-like. Fortunately, for the heavy masses encountered in atomic scattering theory it is usually quite adequate to choose R_m at the equilibrium position R_e defined by the attractive potential $V(R)$, and set the boundary conditions using Eqs. (A6).

The boundary conditions in Eqs. (A6) yield our previous expressions [8] for $\tan\nu=K(t-\gamma)/(t\gamma+K^2)$, $\cot\lambda=K(\gamma-u)/(u\gamma+K^2)$, and $C^{-2}=(s^2K+s'^2/K)$ evaluated at $R=R_e$, where s and s' and the log derivatives $\gamma=f'/f$, $t=\phi'/\phi$, and $u=c'/c$ are obtained from the direct numerical integration of the homogenious $[d^2/dR^2+K^2(\varepsilon,R)]\varphi(\varepsilon,R)=0$. Since at threshold $\varepsilon=0$ the asymptotic boundary condition for both u and t exactly equal zero, $t(0,R)$ and $u(0,R)$ are equivalent at $R=R_e$, and we obtain the required threshold constraint $\tan\lambda(0)=-\cot\nu(0)$. Alternatively we can integrate the nonlinear Milne equation (A3) and numerically evaluate Eq. (A5). Both methods give identical results, and, by definition, $\nu(\varepsilon_n)=n\pi$ will *always* yield exact eigenvalues. However, of even more importance, the resultant bound-state phase $\nu(\varepsilon)$ in Eq. (A5) is a very monotonic, smoothly varying function of ε that can be easily interpolated over wide excursions in energy.

The numerical procedure we use with the Milne equation is as follows. First the f and g functions are evaluated using $\alpha(\varepsilon,R)$ obtained from integrating Eq. (A3). The propagation is generally started at the minimum R_e of the potential well, where the WKB-like initial conditions in Eq. (A6) are well satisfied. Separate inward (from R_e to $R_{\min}$) and outward (from R_e to $R_{\max}$) propagations are performed to obtain the amplitude $\alpha(\varepsilon,R)$ at all R. The accumulated phase $\beta(\varepsilon,R)$ in Eq. (A4) is then obtained by numerical integration. As shown in Eq. (A5) the critical GMQDT parameter for closed channels $\nu(\varepsilon)$ is nothing else than $\beta(\varepsilon,\infty)$. However, in evaluating the other GMQDT parameters one must be careful in using the Milne method for very low asymptotic energies where centrifugal barriers associated with $l>0$ potentials must be penetrated. Under these conditions Lee and Light [34] showed that *spurious* oscillations of $\alpha(\varepsilon,R)$ can occur at distances $R>R_{\text{top}}$ beyond the centrifugal barrier peak at $R=R_{\text{top}}$. To bypass this difficulty Lee and Light split the space into two regions, to the left and right of the barrier. The functions f and g at $R\leqslant R_{\text{top}}$ are determined exactly as described above. For $R>R_{\text{top}}$ an intermediate pair of reference functions $f_\infty=\alpha_\infty\sin\beta_\infty$ and $g_\infty=\alpha_\infty\cos\beta_\infty$ are obtained by propagating *inward* from some large distance $R_{\max}$ using a second solution $\alpha_\infty(R)$ to the Milne equation defined by the asymptotic boundary condition

$$\alpha_\infty(R_{\max})=1/\sqrt{K(R_{\max})}\to 1/\sqrt{k_\infty} \tag{A7}$$

in place of Eq. (A6), and

$$\beta_\infty(\varepsilon,R)=\int_{R_{top}}^{R} dR'/\alpha_\infty^2(\varepsilon,R') \tag{A8}$$

in place of Eq. (A4). This insures that f_∞ and g_∞ are well behaved at long range, and can be asymptotically matched to spherical Bessel functions

$$f_\infty(\varepsilon,R)\underset{R\to\infty}{\sim}(\cos\delta_\infty)J(\varepsilon,R)+(\sin\delta_\infty)N(\varepsilon,R), \tag{A9a}$$

$$g_\infty(\varepsilon,R)\underset{R\to\infty}{\sim}-(\sin\delta_\infty)J(\varepsilon,R)+(\cos\delta_\infty)N(\varepsilon,R). \tag{A9b}$$

By imposing continuity on both sets of functions and their derivatives at $R=R_{\text{top}}$, we can obtain a numerically reliable representation of the analytic reference functions for $R>R_{\text{top}}$:

$$f(\varepsilon,R)=af_\infty(\varepsilon,R)+bg_\infty(\varepsilon,R),\quad R\geqslant R_{\text{top}}, \tag{A10a}$$

$$g(\varepsilon,R)=cf_\infty(\varepsilon,R)+dg_\infty(\varepsilon,R),\quad R\geqslant R_{\text{top}}, \tag{A10b}$$

and easily obtain the required GMQDT parameters. For instance, matching Eq. (A10a) to Eqs. (3.6a) and (3.7a), we find $C(E)=\sqrt{a^2+b^2}$ and $\tan\xi=(a\sin\delta_\infty-b\cos\delta_\infty)/(a\cos\delta_\infty-b\sin\delta_\infty)$. Given C and ξ it is then an easy matter to match Eq. (A10b) to Eqs. (3.6b) and (3.7), and obtain $\tan\lambda=(aC^{-2}-d)/b$. It should be pointed out that even for s-wave scattering some caution must be taken at threshold to avoid spurious oscillations in $\alpha(\varepsilon,R)$ at large distances. Again we can chose an arbitrary R_{top} for $l=0$, using, for example, the same R_{top} defined by the corresponding $l=1$ reference potential, and perform the same matching in Eqs. (A10).

APPENDIX B: NUMERICAL ANALYSIS OF $\mathbf{Y}(R,E)$

In this appendix we describe how the $\mathbf{Y}$ matrix and its R variation is obtained in both diabatic and adiabatic representations. In both cases the set of close-coupled equations (2.2) are propagated in the diabatic representation using a variant of the renormalized Numerov (RN) method implemented by Johnson [35]. As explained by Johnson, the ratio matrix $\mathbf{R}$ which is propagated in the RN method can be replaced by a log-derivative matrix $\mathbf{L}$. Again the diabatic log-derivative matrix $\mathbf{L}$ is obtained. Let us first explain how the diabatic matrix $\mathbf{Y}_d$ is extracted from the close coupling. For a given energy E the diabatic close-coupled wave function $\mathbf{F}_d$ is analyzed with the diabatic reference functions defined by the diagonal interaction matrix elements $W_{ii}(R)$,

$$\mathbf{F}_d(R)=[f_d(R)-g_d(R)\mathbf{Y}_d(R)]\mathbf{A}_d(R), \tag{B1a}$$

$$\mathbf{F}'_d(R)=[f'_d(R)-g'_d(R)\mathbf{Y}_d(R)]\mathbf{A}_d(R), \tag{B1b}$$

where $\mathbf{F}_d$, $\mathbf{Y}_d$, and $\mathbf{A}_d$ are full $N\times N$ square matrices, and f_d and g_d are diagonal matrices. Since, by definition,

$$\mathbf{L}_d(R)=\mathbf{F}'_d(R)\mathbf{F}_d(R)^{-1}, \tag{B2}$$

we find

$$\mathbf{Y}_d(R)=[\mathbf{L}_d(R)_{gd}(R)-g'_d]^{-1}[\mathbf{L}_d(R)f_d(R)-f'_d]. \tag{B3}$$

This analysis is qualitatively similar to the one made in standard scattering theory to extract the $\mathbf{K}_{OO}$ collision matrix, except it is performed at each R value using the diabatic reference functions f_d and g_d in place of the asymptotic Bessel functions J and N, and more fundamentally the complete $N\times N$ matrices $\mathbf{F}_d(R)$ and $\mathbf{Y}_d(R)$ are obtained using both open and closed channels.

Let us now explain how the adiabatic log-derivative matrix $\mathbf{L}_a$ can be derived from $\mathbf{L}_d$. As described in Ref. [8], we introduce the adiabatic wave function $\mathbf{F}_a=\mathbf{M}(R)\mathbf{F}_d(R)$, which can be shown to have the structure

$$\mathbf{M}(R)\mathbf{F}_d(R)=[f_a(R)-g_a(R)\mathbf{Y}_a(R)]\mathbf{A}_a(R), \tag{B4a}$$

$$\mathbf{M}(R)\mathbf{F}'_d(R)=[f'_a(R)-g'_a(R)\mathbf{Y}_a(R)]\mathbf{A}_a(R), \tag{B4b}$$

where $\mathbf{M}(R)$ is the orthogonal matrix which either completely or partially diagonalizes the diabatic interaction matrix $\mathbf{W}(R)=\mathbf{M}(R)\mathbf{V}^O(R)\tilde{\mathbf{M}}(R)$, and produces the matrix $\mathbf{V}^O$ whose diagonal elements define the adiabatic reference functions f_a and g_a. Using Eq. (B4) we can construct an adiabatic log-derivative as follows:

$$\mathbf{L}_a(R)=\mathbf{M}(R)\mathbf{L}_d(R)\tilde{\mathbf{M}}(R) \tag{B5a}$$

$$\equiv[f'_a(R)+g'_a(R)\mathbf{Y}_a(R)][f_a(R)+g_a(R)\mathbf{Y}_a(R)]^{-1}. \tag{B5b}$$

Thus, given $\mathbf{L}_a(R)$ obtained from the CC calculation at each R, we can extract the adiabatic $\mathbf{Y}_a(R)$ matrix as follows:

$$\mathbf{Y}_a(R)=[\mathbf{L}_a(R)g_a(R)-g'_a(R)]^{-1}[\mathbf{L}_a(R)f_a(R)-f'_a(R)]. \tag{B6}$$

[1] See a review by J. Weiner, V. S. Bagnato, S. Zilio, and P. S. Julienne, Rev. Mod. Phys. **71**, 1 (1999).

[2] C. D. Wallace, T. P. Dinneen, K.-Y. N. Tan, T. T. Grove, and P. L. Gould, Phys. Rev. Lett. **69**, 897 (1992); T. Walker, P. Feng, D. Hoffman, and R. S. Williamson III, *ibid.* **69**, 2168 (1992); M. H. Anderson, J. R. Ensher, M. R. Mathhews, C. E. Weiman, and E. A. Cornell, Science **269**, 198 (1995); K. B. Davis, M. O. Mewes, M. R. Andrews, N. J. van Druten, D. S. Durfee, D. M. Kurn, and W. Ketterle, Phys. Rev. Lett. **75**, 3969 (1995).

[3] R. M. C. Ahn, J. P. H. W. v. d. Eijnde, and B. J. Verhaar, Phys. Rev. B **27**, 5424 (1983); H. T. C. Stoof, J. M. V. A. Koelman, and B. J. Verhaar, *ibid.* **38**, 4688 (1988); E. Tiesinga, A. J. Moerdijk, B. J. Verhaar, and H. T. C. Stoof, Phys. Rev. A **46**, R1167 (1992).

[4] F. H. Mies, C. J. Williams, P. S. Julienne, and M. Krauss, J. Res. Natl. Inst. Stand. Technol. **101**, 521 (1996).

[5] P. S. Julienne, F. H. Mies, E. Tiesinga, and C. Williams, Phys. Rev. Lett. **78**, 1880 (1997); P. Leo, E. Tiesinga, P. S. Julienne, D. K. Walter, S. Kadlecek, and T. G. Walker, *ibid.* **81**, 1389 (1998).

[6] E. Tiesinga, B. J. Verhaar, and H. T. C. Stoof, Phys. Rev. A **47**, 4114 (1993); A. J. Moerdijk, B. J. Verhaar, and A. Axelsson, *ibid.* **51**, 3852 (1995); P. Courteille, R. S. Freeland, D. J. Heinzen, F. A. van Abeelen, and B. J. Verhaar, Phys. Rev. Lett. **81**, 69 (1998); S. M. Inouye, R. Andrews, J. Stenger, H.-J. Miesner, D. M. Stamper-Kurn, and W. Ketterle, Nature (London) **392**, 151 (1998); J. Stenger, S. M. Inouye, M. R. Andrews, H.-J. Miesner, D. M. Stamper-Kurn, and W. Ketterle, Phys. Rev. Lett. **82**, 2422 (1998); F. A. van Abeelen and B. J. Verhaar, *ibid.* **83**, 1550 (1999); F. H. Mies, P. Julienne, and E. Tiesinga, Phys. Rev. A **61**, 022721 (2000).

[7] R. J. Napolitano, R. J. Weiner, and P. S. Julienne, Phys. Rev. A **55**, 1191 (1997); P. S. Julienne, J. Res. Natl. Inst. Stand. Technol. **101**, 521 (1996); J. L. Bohn and P. S. Julienne, Phys. Rev. A **60**, 414 (1999); **56**, 1486 (1997).

[8] F. H. Mies, J. Chem. Phys. **80**, 2514 (1984).

[9] F. H. Mies and P. S. Julienne, J. Chem. Phys. **80**, 2526 (1984).

[10] M. Raoult and G. G. Balint-Kurti, J. Chem. Phys. **93**, 6508 (1990).

[11] I. Fourré and M. Raoult, J. Chem. Phys. **101**, 8709 (1994).

[12] J. P. Burke, C. H. Greene, and J. L. Bohn, Phys. Rev. Lett. **81**, 3355 (1998).

[13] M. Arndt, M. Ben Dahan, D. Guery-Odelin, N. W. Reynolds, and J. Dalibard, Phys. Rev. Lett. **79**, 625 (1997).

[14] N. F. Mott and H. S. W. Massey, *The Theory of Atomic Collisions*, 3rd ed. (Oxford University Press, London, 1963).

[15] M. J. Seaton, Proc. Phys. Soc. London **88**, 801 (1966); M. J. Seaton, J. Phys. B **11**, 4067 (1978).

[16] Ch. Jungen, *Molecular Applications of Quantum Defect*

Theory (Institute of Physics, London, 1996).
[17] F. H. Mies, Mol. Phys. **41**, 953 (1980); **41**, 973 (1980).
[18] M. Foucrault, Ph. Millie, and J. P. Daudley, J. Chem. Phys. **96**, 1257 (1992); M. Krauss and W. J. Stevens, *ibid.* **93**, 4236 (1990); M. Marinescu and A. Dalgarno, Phys. Rev. A **52**, 311 (1995).
[19] W. J. Meath, J. Chem. Phys. **45**, 4519 (1966).
[20] We use the convention that boldface symbols represent full matrices that may or may not contain off-diagonal elements, while all other symbols represent either a perfectly diagonal matrix or simply a scaler quantity. Thus $\mathbf{F}=\{F_{i',i}\}$ and $f(\varepsilon,R)=\{f_i(\varepsilon_i,R)\delta_{i',i}\}$, and a scaler such as E in Eq. (2.2) implies $E=E\delta_{i',i}$.
[21] C. H. Greene, U. Fano, and G. Strinati, Phys. Rev. A **19**, 1485 (1979); C. H. Greene and A. R. P. Rau, *ibid.* **26**, 2441 (1982); **30**, 3321 (1984).
[22] B. Gao, Phys. Rev. A **58**, 4222 (1998).
[23] G. F. Gribakin and V. V. Flambaum, Phys. Rev. A **48**, 546 (1993).
[24] V. V. Flambaum, G. F. Gribakin, and C. Harabati, Phys. Rev. A **59**, 1998 (1999).
[25] P. S. Julienne and F. H. Mies, J. Phys. B **14**, 4335 (1981).
[26] F. H. Mies and J. S. Julienne (unpublished).
[27] A. R. P. Rau, Phys. Rev. A **38**, 2255 (1988).
[28] Y. Band and F. H. Mies, J. Chem. Phys. **88**, 2309 (1988); R. Dubs, P. S. Julienne, and F. H. Mies, *ibid.* **93**, 8784 (1990); R. Dubs and P. S. Julienne, *ibid.* **95**, 4177 (1991).
[29] G. Herzberg, *Spectra of Diatomic Molecules*, 2nd ed. (Van Nostrand, Princeton, 1950).
[30] F. H. Mies, Phys. Rev. A **7**, 942 (1973); **7**, 957 (1973).
[31] R. Gordon, J. Chem. Phys. **51**, 14 (1969); Methods Comput. Phys. **10**, 81 (1971).
[32] A. Dalgarno and M. R. H. Rudge, Proc. R. Soc. London, Ser. A **286**, 519 (1965); H. O. Dickinson and M. R. H. Rudge, J. Phys. B **3**, 1448 (1970).
[33] S.-H. Pan and F. H. Mies, J. Chem. Phys. **89**, 3096 (1988).
[34] S.-Y. Lee and J. C. Light, Chem. Phys. Lett. **25**, 435 (1974).
[35] B. R. Johnson, J. Chem. Phys. **69**, 3678 (1978).
[36] R. Shakeshaft, J. Phys. B **5**, L115 (1972).
[37] H. R. Sadeghpour *et al.*, J. Phys. B **33**, R93 (2000).